

Diffusion posterior sampling for simulation-based inference in tall data settings

Julia Linhart[‡], Gabriel Victorino Cardoso^{*}, Alexandre Gramfort^{*}, Sylvain Le Corff[†], and
Pedro L. C. Rodrigues^{II}

[‡]Université Paris-Saclay, Inria, CEA.

^{*}CMAP, École Polytechnique, Institut Polytechnique de Paris.

^{*}Université Paris-Saclay, Inria, CEA.

[†]LPSM, Sorbonne Université, UMR CNRS 8001.

^{II}Univ. Grenoble Alpes, Inria, CNRS, Grenoble INP, LJK.

Abstract

Determining which parameters of a non-linear model best describe a set of experimental data is a fundamental problem in science and it has gained much traction lately with the rise of complex large-scale simulators. The likelihood of such models is typically intractable, which is why classical MCMC methods can not be used. Simulation-based inference (SBI) stands out in this context by only requiring a dataset of simulations to train deep generative models capable of approximating the posterior distribution that relates input parameters to a given observation. In this work, we consider a *tall data* extension in which multiple observations are available to better infer the parameters of the model. The proposed method is built upon recent developments from the flourishing score-based diffusion literature and allows to estimate the *tall data posterior* distribution, while simply using information from a score network trained for a *single context observation*. We compare our method to recently proposed competing approaches on various numerical experiments and demonstrate its superiority in terms of numerical stability and computational cost.

1 Introduction

Inverting non-linear models describing natural phenomena is a fundamental problem in science and has been tackled by many fields (Gonçalves et al., 2020; Dax et al., 2023). In this work, we consider a Bayesian approach in which the input parameters $\theta \in \mathbb{R}^m$ of a model \mathcal{M} that best explain a set of output observations $x \in \mathbb{R}^d$ are described via a posterior distribution $p(\theta | x)$. Obtaining samples of the posterior can, however, be very challenging when the outputs of \mathcal{M} are obtained through complex simulations (e.g. solutions of non-linear differential equations). Indeed, in these cases the likelihood $p(x | \theta)$ is often impossible to evaluate and MCMC procedures cannot be used.

Simulation-based inference (SBI) (Cranmer et al., 2020) is a promising approach that bypasses the difficulties of likelihood evaluations via simulations from the model and leverages the recent advances from deep generative learning. The procedure relies on the choice of a prior distribution $\lambda(\theta)$ encoding knowledge

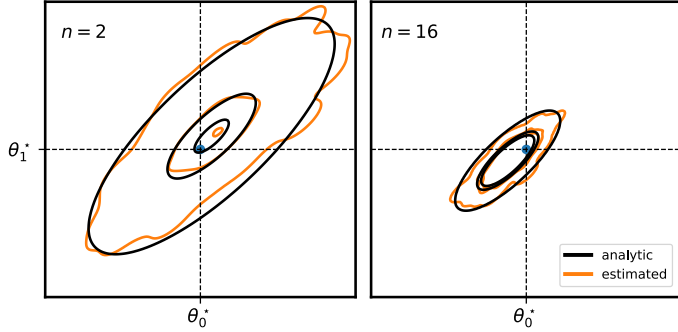


Figure 1: The posterior distribution of a model with a Gaussian simulator and Gaussian prior concentrates around the **true parameter** θ^* as the number n of observations $x_i \sim p(x | \theta^*)$ increases. In this simple setting we can calculate the **analytic** posterior distribution and compare it to the posterior **estimated** with our score-based proposal (**GAUSS**).

about the values of \mathcal{M} 's parameters and a simulated dataset generated as:

$$\Theta_i \sim \lambda(\theta), \quad X_i \sim p(x | \Theta_i), \quad (\Theta_i, X_i) \sim p(\theta, x).$$

Let N_s be a fixed simulation budget, we can sample a dataset $\mathcal{D} = \{(\Theta_i, X_i)\}_{i=1}^{N_s}$ and train conditional deep generative models to generate samples from $p(\theta | x^*)$ for any new observation x^* . Usual approaches target either the posterior directly (NPE) (Greenberg et al., 2019), the likelihood function (NLE) (Papamakarios et al., 2019), or the likelihood-to-evidence ratio (NRE) (Hermans et al., 2020). In NPE, the posterior samples can be obtained directly by sampling a conditional normalizing flow (Papamakarios et al., 2021), whereas in NLE and NRE additional MCMC sampling is required.

In this work, we consider a natural extension of the above Bayesian framework to the *tall data* setting (Bardenet et al., 2015), in which multiple observations $x_{1:n}^* = (x_1, \dots, x_n)$ are available and

$$p(\theta | x_{1:n}^*) \propto \lambda(\theta)^{1-n} \prod_{j=1}^n p(\theta | x_j^*), \quad (1)$$

the *tall data* posterior, is expected to provide more precise information about how to invert \mathcal{M} (see Fig 1). While this framework is crucial for practical applications, there is no satisfactory solution to process such a *tall data* setting in SBI procedures. In Rodrigues et al. (2021), the authors merge a fixed number of extra observations via a Deepset (Zaheer et al., 2017) and fall back to NPE trained on an augmented dataset with samples $\mathcal{D}_n = \{(\Theta_i, X_{i,1:n})\}$. Important drawbacks of this approach are the potentially heavy cost of generating extra observations via the simulator ($N_s^{\text{aug}} = N_s \times n$) and the lack of flexibility on the number of extra observations at inference time. In Hermans et al. (2020), the authors show how the amortization of NRE allows to handle the *tall data* setting *without requiring new simulations or retraining*, by factorizing over the set of multiple observations. An equivalent extension can be done for NLE (Geffner et al., 2023). Note, however, that both approaches still require a MCMC sampler to obtain posterior samples, which is often undesirable in SBI applications.

Recently, Sharrock et al. (2022) proposed a new method that relies on score-based generative modelling (SBGM) (Ho et al., 2020; Song et al., 2021b) to approximate the posterior distribution targeted in SBI, called *Neural Posterior Score Estimation* (NPSE). It introduces an easy-to-train objective to learn the *score* $\nabla_{\theta} \log p_t(\theta | x)$ of a sequence of noisy versions of the target distribution, using the simulated dataset \mathcal{D} . Sampling from the posterior then consists in progressively denoising the perturbed data by solving the backward diffusion process using the learned score. SBGM rivals state-of-the-art generative models such as generative adversarial networks (GANs) (Goodfellow et al., 2014) and normalizing flows (Papamakarios

et al., 2021) in challenging high-dimensional datasets, without the need of adversarial training or special (e.g. invertible) network architectures. Indeed, NPSE trained with transformer architectures is currently the most flexible SBI algorithm and achieves state-of-the-art performance on benchmark tasks, as recently shown by Gloeckler et al. (2024).

However, extending NPSE to the *tall data* setting is challenging, as a direct application of the method would require training a score network $s_\phi(\theta, x_{1:n}, t)$ to approximate $\nabla_\theta \log p_t(\theta | x_{1:n})$ on an augmented dataset \mathcal{D}_n , which leads to the same drawbacks as for the augmented NPE approach. Geffner et al. (2023) recently proposed F-NPSE that, like Hermans et al. (2020) for NRE, exploits the amortization of NPSE to approximate the *tall data* posterior without the need of an augmented dataset or retraining the score network. To do so, F-NPSE introduces a sequence of distributions for which the score can be computed by composing *individual scores* $s_\phi(\theta, x_j, t)$ obtained for each observation x_j , following the *factorization* from Equation (1). The major drawback of this approach, however, is that the diffusion process followed by this sequence is unknown, which reintroduces the need of MCMC methods to sample from the posterior via an annealed Langevin procedure.

In this paper, we propose a new sampling algorithm that approximates the *tall data* posterior using only the *individual scores* obtained from an amortized NPSE, but *without the need of Langevin dynamics*, by directly solving the backward diffusion process for the tall posterior using the factorization from Equation (1). This sampler relies on a second order approximation of the backward diffusion kernels associated with the individual posterior scores. We demonstrate the superiority of our approach as compared to F-NPSE on several numerical experiments: two Gaussian toy models for which all quantities of interest are known analytically, three examples from the SBI benchmark, and the inversion of a challenging model from computational neuroscience.

2 Background

Score based generative models (SBGM). The goal of SBGM is to estimate an *unknown* target data distribution q_{data} from samples $\theta_1, \dots, \theta_M \in \mathbb{R}^d \sim_{\text{iid}} q_{\text{data}}$ with the help of a *forward* diffusion process that adds noise to the training data. The main idea is to approximately sample the target distribution by solving the associated *backward* diffusion process. This procedure requires to approximate the score functions of the diffused data distributions for different levels of added noise.

In this work, we focus on the variance preserving (VP) framework (Ho et al., 2020; Yang et al., 2023) in which a sequence of noisy versions $\{\theta_t\}_{t \in [1:T]}$ of q_{data} is defined for $t \in [1 : T]$, by

$$\theta_t = \sqrt{\alpha_t} \theta_0 + \sqrt{1 - \alpha_t} \epsilon_t,$$

where $\theta_0 \sim q_{\text{data}}$, $\{\epsilon_t\}_{t \in [1:T]}$ are i.i.d. with distribution $\mathcal{N}(0, \mathbf{I}_m)$ and $\{\alpha_t\}_{t \in [1:T]} \in [0, 1]^T$ is a decreasing sequence of positive real numbers. Let $q_{t|0}(\theta_t | \theta_0) = \mathcal{N}(\theta_t; \sqrt{\alpha_t} \theta_0, (1 - \alpha_t) \mathbf{I}_m)$ be the probability density function of the conditional distribution of θ_t given θ_0 and q_t the density of θ_t . Following Hyvärinen and Dayan (2005); Vincent (2011), we can learn the score of q_t via a neural network s_ψ by minimising $\mathcal{L} : \psi \mapsto \mathbb{E}_{\theta_t \sim q_t} [\|s_\psi(\theta_t, \alpha_t) - \nabla \log q_t(\theta_t)\|^2]$ without knowledge of the ground-truth data score. Using Fisher’s identity, we can define the denoising score-matching loss

$$\mathcal{L}_{\text{score}}(\psi) = \sum_{t=1}^T \gamma_t^2 \mathbb{E}_{\theta_0 \sim q_{\text{data}}, \theta_t \sim q_{t|0}(\cdot | \theta_0)} \left[\|s_\psi(\theta_t, \alpha_t) - \nabla \log q_{t|0}(\theta_t | \theta_0)\|^2 \right], \quad (2)$$

where γ_t is a positive weighting function introduced in Vincent (2011).

Once we have the score approximation $s_\psi(\theta_t, \alpha_t)$ of $\nabla \log q_t(\theta_t)$, the goal is to draw *backwards* starting from $\theta_T \sim q_T$ to obtain samples approximately distributed according to q_{data} at time 0. Different ways to perform this backward sampling include the use of annealed Langevin dynamics (Song and Ermon, 2019), stochastic differential equations (Song et al., 2021b), or ordinary differential equations (Kararas et al., 2022). In this work, we follow the approach proposed in Song et al. (2021a), which yields the denoising diffusion implicit models (DDIM) sampler. DDIM introduces a set of inference distributions indexed by $\sigma = \{\sigma_t \in (0, \alpha_t^{1/2})\}_{t \in [1:T-1]}$ defined for $t \in [1 : T - 1]$ as $q_{t|t+1,0}^\sigma(\theta_t|\theta_0, \theta_{t+1}) = \mathcal{N}(\theta_{t-1}; \boldsymbol{\mu}_t(\theta_0, \theta_t), \sigma_t^2 \mathbf{I}_m)$, with $\boldsymbol{\mu}_t(\theta_0, \theta_t) = \alpha_{t-1}^{1/2} \theta_0 + (v_{t-1} - \sigma_t^2)^{1/2} (\theta_t - \alpha_t^{1/2} \theta_0) / (1 - \alpha_t)^{1/2}$. Note that $\boldsymbol{\mu}_t$ is chosen so that $q_{t|0}^\sigma(\theta_t|\theta_0) = \mathcal{N}(\theta_t; \sqrt{\alpha_t} \theta_0, (1 - \alpha_t) \mathbf{I}_m)$ (Song et al., 2021a, Lemma 1, Appendix B). This property allows us to write $q_{t-1}(\theta_{t-1}) = \int q_{t-1|t,0}^\sigma(\theta_{t-1}|\theta_t, \theta_0) q_{0|t}(\theta_0|\theta_t) q_t(\theta_t) d\theta_0 d\theta_t$. Even though the equation above suggests a way of passing from q_t to q_{t-1} , it involves an intractable kernel $\int q_{t-1|t,0}^\sigma(\theta_{t-1}|\theta_t, \theta_0) q_{0|t}(\theta_0|\theta_t) d\theta_0$. The marginal distribution can be approximated by

$$\hat{q}_{t-1}(\theta_{t-1}) = \int q_{t-1|t,0}^\sigma(\theta_{t-1}|\theta_t, \mu_t(\theta_t)) q_t(\theta_t) d\theta_t, \quad (3)$$

where $\mu_t(\theta_t) := \mathbb{E}_{\theta_0 \sim q_{0|t}^\sigma(\cdot|\theta_t)}[\theta_0]$, and verifies

$$\alpha_t^{1/2} \mu_t(\theta_t) - \theta_t = (1 - \alpha_t) \mathbb{E}_{\theta_0 \sim q_{0|t}^\sigma(\cdot|\theta_t)}[\nabla \log q_{t|0}(\theta_t|\theta_0)].$$

Using (2), we can now define the following approximation of $\mu_t(\theta_t)$ for all $t \in [1 : T]$

$$\mu_{\psi,t}(\theta_t) := \alpha_t^{1/2} \left(\theta_t + (1 - \alpha_t) s_\psi(\theta_t, \alpha_t) \right). \quad (4)$$

We finally obtain the following backward Markov chain for DDIM:

$$p_{\psi,0:T}(\theta_{0:T}) = p_T(\theta_T) \prod_{t=1}^T p_{\psi,t-1|t}(\theta_{t-1}|\theta_t), \quad (5)$$

where $p_T(\theta_T) = q_T(\theta_T)$, $p_{\psi,t-1|t}(\theta_{t-1}|\theta_t) = q_{t-1|t,0}^\sigma(\theta_{t-1}|\theta_t, \mu_{\psi,t}(\theta_t))$ and $p_{\psi,0|1}(\theta_0|\theta_1) = \mathcal{N}(\theta_0; \mu_{\psi,1}(\theta_1), \sigma_0^2 \mathbf{I}_m)$, with $\sigma_0 > 0$ a free parameter.

Factorized neural posterior score estimation. The F-NPSE method proposed in Geffner et al. (2023) defines a sequence of distributions $\{\varrho_t(\cdot | x)\}_{t \in [0:T]}$ such that

$$\nabla_\theta \log \varrho_t(\theta | x_{1:n}^*) = (1 - n)(1 - t) \nabla_\theta \log \lambda(\theta) + \sum_{j=1}^n s_\psi(\theta, x_j, \alpha_t), \quad (6)$$

where the score of ϱ_0 is the score of the tall posterior defined in (1). F-NPSE uses Langevin dynamics to sample ϱ_t for each $t = T, \dots, 0$ and has shown superior performance as compared to all competing methods for *tall data* settings (i.e. augmented or factorized versions of NPE, NLE, and NRE) in terms of posterior reconstruction, achieving the best trade-off between sample efficiency and accumulation of errors when the number of observations grows. The main limitation of F-NPSE is the use of Langevin dynamics, which can be very sensitive to the choices of step-size at each sampling iteration, as well as the total number of steps. We justify these claims with empirical results in Section 4.1 and Appendix K.

3 Diffusion posterior sampling for tall data

In this section, we propose a new algorithm that approximately samples from the backward diffusion process associated with the factorized tall data posterior, thereby eliminating the need of costly and unstable Langevin steps, while using only individual scores obtained for each observation.

3.1 Exact computation of the tall data posterior score

Let $x_{1:n}^* = \{x_1^*, \dots, x_n^*\} \sim_{\text{iid}} p(x | \theta^*)$ be observations sampled using the same parameter $\theta^* \in \mathbb{R}^m$. Our goal is to sample from the *tall data* posterior $p(\theta | x_{1:n}^*)$ via the backward sampling Markov chain defined in (5), while only relying on a score estimate $s_\phi(\theta, x, \alpha_t) \approx \nabla_\theta \log p_t(\theta | x)$ of the diffused posterior for a single observation x . To do so, we need to build an approximation of the diffused *tall data* posterior score $\nabla_{\theta_t} \log p_t(\theta_t | x_{1:n}^*) = \nabla_{\theta_t} \log \int p(\theta | x_{1:n}^*) q_{t|0}(\theta_t | \theta) d\theta$ that solely depends on $\nabla_\theta \log p_t(\theta | x_j^*)$, for all $j \in [1, n]$. Using (1) we can write

$$p_t(\theta | x_{1:n}^*) = \int p(\theta_0 | x_{1:n}^*) q_{t|0}(\theta | \theta_0) d\theta_0 \propto \int \left(\lambda(\theta_0)^{1-n} \prod_{j=1}^n p(\theta_0 | x_j^*) \right) q_{t|0}(\theta | \theta_0) d\theta_0. \quad (7)$$

Given the diffused prior $p_t^\lambda(\theta) = \int \lambda(\theta_0) q_{t|0}(\theta | \theta_0) d\theta_0$, we now introduce the following backward transition kernels obtained via Bayes' rule:

$$p_{0|t}(\theta_0 | \theta, x) = \frac{p(\theta_0 | x) q_{t|0}(\theta | \theta_0)}{p_t(\theta | x)} \quad \text{and} \quad p_{0|t}^\lambda(\theta_0 | \theta) = \frac{\lambda(\theta_0) q_{t|0}(\theta | \theta_0)}{p_t^\lambda(\theta)}. \quad (8)$$

Rearranging terms in Equation (7) and using (8) yields

$$\begin{aligned} p_t(\theta | x_{1:n}^*) &\propto \int (\lambda(\theta_0) q_{t|0}(\theta | \theta_0))^{1-n} \prod_{j=1}^n p(\theta_0 | x_j^*) q_{t|0}(\theta | \theta_0) d\theta_0 \\ &= L_\lambda(\theta, x_{1:n}^*) p_t^\lambda(\theta)^{1-n} \prod_{j=1}^n p_t(\theta | x_j^*), \end{aligned}$$

with $L_\lambda(\theta, x_{1:n}^*) := \int p_{0|t}^\lambda(\theta_0 | \theta)^{1-n} \prod_{j=1}^n p_{0|t}(\theta_0 | \theta, x_j^*) d\theta_0$. The corresponding score writes

$$\nabla_\theta \log p_t(\theta | x_{1:n}^*) = (1-n) \nabla_\theta \log p_t^\lambda(\theta) + \sum_{j=1}^n \nabla_\theta \log p_t(\theta | x_j^*) + \nabla_\theta \log L_\lambda(\theta, x_{1:n}^*).$$

The first two terms in the above equation are tractable: the prior score can be computed analytically in most cases¹ and the (single) posterior scores are approximated by evaluating the learned score model $s_\phi(\theta, x, \alpha_t)$ at every x_j^* . This leaves the last term that integrates all backward kernels for each x_j^* which needs to be estimated. Note that this term is missing in the score formula from Equation (6) and is the reason why Langevin steps are required in F-NPSE.

¹See Appendix D for the Gaussian and Uniform cases. If not, it can be learned via the classifier-free guidance approach (Ho and Salimans, 2021), at the same time as the posterior score (more details and experimental results are provided in Appendix L.1)

3.2 Second order approximation of $\log L_\lambda$

We consider a Gaussian approximation of the backward kernels defined in (8) via

$$\hat{p}_{0|t}(\theta_0|x) = \mathcal{N}(\theta_0; \mu_t(\theta, x), \Sigma_t(\theta, x)) \quad \text{and} \quad \hat{p}_{0|t}^\lambda(\theta_0|\theta) = \mathcal{N}(\theta_0; \mu_{t,\lambda}(\theta), \Sigma_{t,\lambda}(\theta)), \quad (9)$$

where $\mu_t(\theta, x)$, $\mu_{t,\lambda}(\theta)$ and $\Sigma_t(\theta, x)$, $\Sigma_{t,\lambda}(\theta)$ are the means and covariance matrices of the backward processes respectively associated with the diffused posterior $p_t(\theta | x)$ and prior $p_t^\lambda(\theta)$ distributions.² This leads us to the following estimator of $\log L_\lambda(\theta, x_{1:n}^*)$:

$$\ell_\lambda(\theta, x_{1:n}^*) = \log \int \hat{p}_{0|t}^\lambda(\theta_0|\theta)^{1-n} \prod_{j=1}^n \hat{p}_{0|t}(\theta_0|\theta, x_j^*) d\theta_0. \quad (10)$$

From now on, we alleviate the dependency on x_j and write $\mu_{t,j}(\theta) = \mu_{t,j}(\theta, x_j)$ and $\Sigma_{t,j}(\theta) = \Sigma_t(\theta, x_j)$. We now state the two Lemmas that are the foundation of our approximation of the score of the tall posterior. All proofs are postponed to Appendix A.

Lemma 3.1. *For all $\theta \in \mathbb{R}^m$, let $\Lambda(\theta) = \sum_{j=1}^n \Sigma_{t,j}^{-1}(\theta) + (1-n)\Sigma_{t,\lambda}^{-1}(\theta)$. Assume that $\Lambda(\theta)$ is positive definite. Then, for all $\theta \in \mathbb{R}^m$ and $x_j^* \in \mathbb{R}^d$, $1 \leq j \leq n$,*

$$\ell_\lambda(\theta, x_{1:n}^*) = \sum_{j=1}^n \zeta_j(\theta) + (1-n)\zeta_\lambda(\theta) - \zeta_{\text{all}}(\theta), \quad (11)$$

where $\zeta(\mu, \Sigma) = -(m \log 2\pi - \log |\Sigma^{-1}| + \mu^\top \Sigma^{-1} \mu) / 2$, and $\zeta_j(\theta) = \zeta(\mu_{t,j}(\theta), \Sigma_{t,j}(\theta))$ for all $j \in [1 : n]$, $\zeta_\lambda(\theta) = \zeta(\mu_{t,\lambda}(\theta), \Sigma_{t,\lambda}(\theta))$ and $\zeta_{\text{all}}(\theta) = \zeta(\Lambda(\theta)^{-1} \eta(\theta), \Lambda(\theta)^{-1})$ with $\eta(\theta) = \sum_{j=1}^n \Sigma_{t,j}^{-1}(\theta) \mu_{t,j}(\theta) + (1-n)\Sigma_{t,\lambda}^{-1}(\theta) \mu_{t,\lambda}(\theta)$.

Lemma 3.2. *For all $\theta \in \mathbb{R}^m$ and $x_j^* \in \mathbb{R}^d$, $1 \leq j \leq n$, the full gradient can be written as*

$$\begin{aligned} \nabla_\theta \log p_t(\theta | x_{1:n}^*) &= \Lambda(\theta)^{-1} \sum_{j=1}^n \Sigma_{t,j}^{-1}(\theta) \nabla_\theta \log p_t(\theta | x_j^*) \\ &\quad + (1-n)\Lambda(\theta)^{-1} \Sigma_{t,\lambda}^{-1}(\theta) \nabla_\theta \log p_t^\lambda(\theta) + F(\theta, x_{1:n}^*), \end{aligned} \quad (12)$$

where $F(\theta, x_{1:n}^*) = 0$ if $\nabla_\theta \Sigma_{t,j}(\theta) = 0$ for all $1 \leq j \leq n$ and $\nabla_\theta \Sigma_{\lambda,t}(\theta) = 0$.

Formula (12) defines our approximation of the diffused tall posterior score and depends solely on the individual (prior and posterior) scores. We now focus on the computation of the backward covariance matrices $\Sigma_{t,\lambda}(\theta)$ and $\Sigma_{t,j}(\theta)$ with $1 \leq j \leq n$, while keeping in mind that we want $F(\theta, x_{1:n}^*)$ to be zero. First, note that for some prior choices, $\Sigma_{t,\lambda}(\theta)$ can be computed analytically; otherwise, we use the same strategy as for the intractable posterior case. This is represented by `prior_fn` in Algorithms 1 and 2.

From (Boys et al., 2023), it can be shown that $\Sigma_{t,j}(\theta) = \alpha_t^{-1/2} (1 - \alpha_t) \nabla_\theta \mu_{t,j}(\theta)$, where $\mu_{t,j}(\theta_t)$ is completely defined with the posterior score as in Equation (4). $\Sigma_{t,j}(\theta_t)$ can therefore be approximated by directly taking the Jacobian of the learned score function $s_\phi(\theta, x_j^*, \alpha_t)$. As proposed in Boys et al. (2023), we do not propagate gradients through $\Sigma_{t,i}(\theta)$, rendering $F(\theta, x_{1:n}^*) = 0$ in Lemma 3.2. This corresponds

² $\mu_t(\theta) = \mathbb{E}[\theta_0 | \theta]$ and $\Sigma_t(\theta) = \text{Cov}(\theta_0 | \theta)$ are functions of the score and its derivatives Boys et al. (2023).

to Algorithm 2, which we refer to as JAC. But this approach has two main drawbacks. First, we need to calculate a $m \times m$ matrix which is prohibitive for large m . Second, we have to take the derivative w.r.t. the inputs of the score neural network, which is known to be unstable.

As an alternative, we consider a constant approximation of the covariance matrix. To do so, we start by noting that in the case where q_{data} is a Gaussian distribution with mean μ_0 and variance Σ_0 , we have $\Sigma_t = (\Sigma_0^{-1} + \alpha_t(1 - \alpha_t)^{-1}\mathbf{I}_m)^{-1}$, see Appendix D. Note that choosing $\Sigma_0 = \mathbf{I}_m$ results in the approximation proposed by Song et al. (2023). We use the formula for the Gaussian case as an approximation of the real covariance matrix $\Sigma_{t,j}$, yielding Algorithm 1 which we refer to as GAUSS. To do so, we need to first estimate $\Sigma_{0,j}$ for each x_j^* , which we do by first running a DDIM with a small number of iterations (100) for each j and using the empirical covariance matrix of the samples as $\Sigma_{0,j}$. Note that in this case, we also have $F(\theta, x_{1:n}) = 0$ in Lemma 3.2.

Algorithm 1 GAUSS

 (Gaussian approximation)

Input: $\theta, x_{1:n}, t, \hat{\Sigma}_{1:n}, \text{prior_fn}$
Output: $s_{1:n}$
 $\Sigma_{t,\lambda}^{-1}, s_\lambda \leftarrow \text{prior_fn}(\theta, t)$
for $j \leftarrow 1$ to n **do**
 $s_j \leftarrow s_\psi(\theta, x_j, \alpha_t)$
 $\hat{\Sigma}_{t,j}^{-1} \leftarrow \hat{\Sigma}_j^{-1} + \frac{\alpha_t}{(1-\alpha_t)}\mathbf{I}_m$
end for
 $\Lambda \leftarrow (1-n)\Sigma_{t,\lambda}^{-1} + \sum_{i=1}^n \hat{\Sigma}_{t,i}^{-1}$
 $\tilde{s}_{1:n} \leftarrow (1-n)\Sigma_{t,\lambda}^{-1}s_\lambda + \sum_{i=1}^n \hat{\Sigma}_{t,i}^{-1}s_i$
 $s_{1:n} \leftarrow \text{LinSolve}(\Lambda, \tilde{s}_{1:n})$

Algorithm 2 JAC

 (Jacobian approximation)

Input: $\theta, x_{1:n}, t, \text{prior_fn}$
Output: $s_{1:n}$
 $\Sigma_{t,\lambda}^{-1}, s_\lambda \leftarrow \text{prior_fn}(\theta, t)$
for $j \leftarrow 1$ to n **do**
 $s_j \leftarrow s_\psi(\theta, x_j, \alpha_t)$
 $\hat{\Sigma}_{t,j}^{-1} \leftarrow \frac{\alpha_t}{(1-\alpha_t)} (\mathbf{I}_m + (1-\alpha_t)\nabla_{\theta} s_\psi(\theta, x_j, \alpha_t))^{-1}$
end for
 $\Lambda \leftarrow (1-n)\Sigma_{t,\lambda}^{-1} + \sum_{i=1}^n \hat{\Sigma}_{t,i}^{-1}$
 $\tilde{s}_{1:n} \leftarrow (1-n)\Sigma_{t,\lambda}^{-1}s_\lambda + \sum_{i=1}^n \hat{\Sigma}_{t,i}^{-1}s_i$
 $s_{1:n} \leftarrow \text{LinSolve}(\Lambda, \tilde{s}_{1:n})$

4 Experiments

We investigate the performance of GAUSS and JAC for different tasks from the SBI literature with increasing difficulty. We choose F-NPSE (Geffner et al., 2023) as a baseline for comparisons, which uses unadjusted Langevin dynamics (ULD) with $L = 5$ steps and $\tau = 0.5$. We have decided to not compare our methods to augmented versions of NPE, NLE, and NRE because it has already been shown that the score-diffusion framework demonstrates clear superior performance (Sharrock et al., 2022; Geffner et al., 2023; Gloeckler et al., 2024). For GAUSS and JAC we sample with the backward Markov chain defined in Section 2 with $\sigma_t^2 = \eta^2(1 - \alpha_{t-1}) / ((1 - \alpha_t)(1 - \alpha_t / \alpha_{t-1}))$ where $\eta = 0.2, 0.5, 0.8, 1$ for a number of steps $T = 50, 150, 400, 1000$ respectively. We use a uniform scheduling $\{t_i = i/T\}_{i=1}^T$. To evaluate the accuracy of the sampling algorithms, we compute the sliced Wasserstein (sW) distance between estimated and true posterior samples. Further implementation details can be found in Appendix E and the code reproducing all experiments is available in the following repository: <https://github.com/JuliaLinhart/diffusions-for-sbi>.

Algorithm	N steps	Δt (s)	sW
GAUSS	50	0.45 +/- 0.00	0.17 +/- 0.08
JAC	50	0.41 +/- 0.00	3.14 +/- 4.12
LANGEVIN	50	0.83 +/- 0.00	nan +/- nan
GAUSS	150	0.90 +/- 0.00	0.17 +/- 0.06
JAC	150	1.22 +/- 0.00	1.57 +/- 2.33
LANGEVIN	150	2.50 +/- 0.01	0.65 +/- 0.42
GAUSS	400	2.04 +/- 0.00	0.20 +/- 0.11
JAC	400	3.26 +/- 0.01	0.85 +/- 1.20
LANGEVIN	400	6.65 +/- 0.02	0.65 +/- 0.43
GAUSS	1000	4.77 +/- 0.01	0.22 +/- 0.10
JAC	1000	8.18 +/- 0.03	0.25 +/- 0.09
LANGEVIN	1000	16.65 +/- 0.03	0.65 +/- 0.42

Table 1: Sliced Wasserstein (sW) and total elapsed time Δt for the Gaussian toy problem with $m = 10$, $n = 32$ and $\epsilon = 10^{-2}$ per algorithm and number N of sampling steps. Mean and std over 5 different seeds.

4.1 Gaussian toy models

We consider two toy examples for which the analytic form of the posterior and corresponding score distributions are known. Our first example is a multivariate Gaussian simulator $p(x | \theta) = \mathcal{N}(x; \theta, (1 - \rho)\mathbf{I}_m + \rho\mathbf{1}_m)$ with correlation factor $\rho = 0.8$. The second is a Mixture of Gaussians (GMM) $p(x | \theta) = 0.5 \mathcal{N}(x; \theta, 2.25\Sigma) + 0.5 \mathcal{N}(x; \theta, \Sigma/9)$, where Σ is a diagonal matrix with values increasing linearly between 0.6 and 1.4, following [Geffner et al. \(2023\)](#). Both examples are carried out with a Gaussian prior $\lambda(\theta) = \mathcal{N}(\theta; 0, \mathbf{I}_m)$ in dimension $m = 10$. Here, the samples of the true posterior with multiple observations can be obtained either directly for the Gaussian model or via Metropolis Adjusted Langevin (MALA) for GMM (see Appendix E for further details).

Consider the following approximate score model $\tilde{s}_\psi(\theta, x, \alpha_t) = s_\psi(\theta, x, \alpha_t) + \epsilon(1 - \alpha_t)r(\theta, x, \alpha_t)$, where $\epsilon \geq 0$, $s_\psi(\theta, x, \alpha_t)$ is the analytical posterior score and r is a randomly initialized neural net with outputs in range $[-1, 1]$, see Appendix D. This construction leads to an error of ϵ over the “noise predictor” network defined as $-\tilde{s}_\psi(\theta, x, \alpha_t)/(1 - \alpha_t)$, which is the neural network that one actually optimizes when training a score model. Note that unlike the Gaussian case, the Gaussian approximation from section 3.2 is not exact for GMM, i.e. $p_{0|t}(\theta_0|\theta_t)$ is not a Gaussian density for all θ_t and all $t \in [1 : T]$. Therefore, this example allows us to quantify the effect of our approximation while still controlling the score estimation error (through ϵ). The following results evaluate the robustness of the algorithms to increasing error rates ϵ and number of conditioning observations n .

Table 1 displays the total running time and sW³ for each algorithm on the Gaussian example (Table 3 in Appendix G shows similar results for GMM). We can see that for the same number of time steps, our algorithm yields smaller sW than the Langevin sampler while accounting for $L = 5$ times less neural network evaluation, thus 5 times faster. We show in Appendix G the differences in speed for each tested setting. Based on this table, we consider “equivalent time settings”, namely we run our algorithm with 400 and 1000 steps for **JAC** and **GAUSS** respectively and **LANGEVIN** for 400 steps.

Figure 2 portrays the effect of the perturbation ϵ in the posterior approximation for each algorithm for $n \in [1, 100]$. In the Gaussian example we see that **GAUSS** is better in all settings. This is the expected behaviour, since in this example our method based on second order approximations fits perfectly the score of the tall posterior. **JAC** is exact for zero or very small perturbations ($\epsilon = 0, 0.001$), but becomes unstable

³The sW is computed with 10^4 slices on 10^3 samples. To account for finite-sample effects, we considered a normalized version of sW by removing the expected sW over different sample sets from the true distribution.

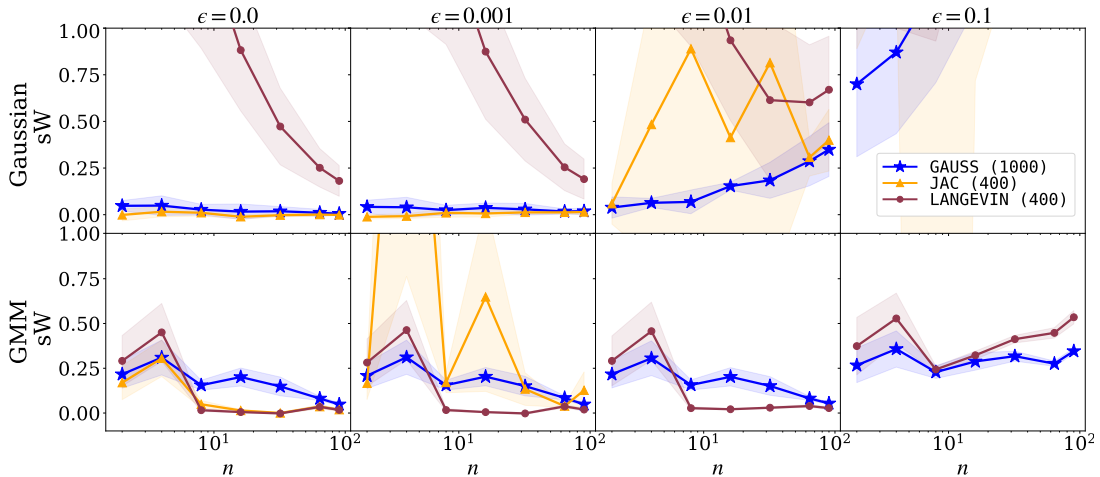


Figure 2: Sliced Wasserstein (sW) distance as a function of the number of observations n for the Gaussian and GMM toy examples, for each algorithm (**GAUSS**, **JAC** and **LANGEVIN**) and with different levels of ϵ . Mean and std over 5 different seeds.

when it increases ($\epsilon = 0.01$). In GMM, our approximation **GAUSS** is competitive with **LANGEVIN**, achieving smaller sW for small n and then reaching the same sW for $n = 90$, while being the best for all n in the setting with the highest amount of perturbation ($\epsilon = 10^{-1}$). We see that **JAC** is extremely precise for $\epsilon = 0$ (which corresponds to the case where the analytical posterior score is available) and becomes unstable for $\epsilon > 0$. This suggests that **GAUSS** offers a good trade-off between precision and robustness and thus the better algorithm choice in SBI settings where the posterior score is unknown and has to be approximated.

We include in Appendix G a complete analysis for the Gaussian example, comparing all algorithms for different choices of dimensions m , number of observations n , and precision ϵ .

4.2 Benchmark SBI examples

We consider three examples from the popular SBI benchmark presented in Lueckmann et al. (2021):

- SLCP ($m = 5$, $d = 8$): Uniform prior and Gaussian simulator, whose mean and covariance are non-linear functions of the input parameters θ .
- SIR ($m = 2$, $d = 10$): Log-Normal prior and simulator based on a set of differential equations that outputs sampled from a Binomial distribution.
- Lotka-Volterra ($m = 4$, $d = 20$): Log-Normal prior and simulator based on a set of differential equations that outputs sampled from a Log-Normal distribution.

The score corresponding to each prior distribution is analytically computable; see Appendix D. However, contrarily to the toy models considered in Section 4.1, the analytical posterior score is not available for the chosen examples and is, therefore, learned via score-matching as explained in Section 2. The goal of this experiment is to evaluate the robustness of the different sampling algorithms to this learning setting.

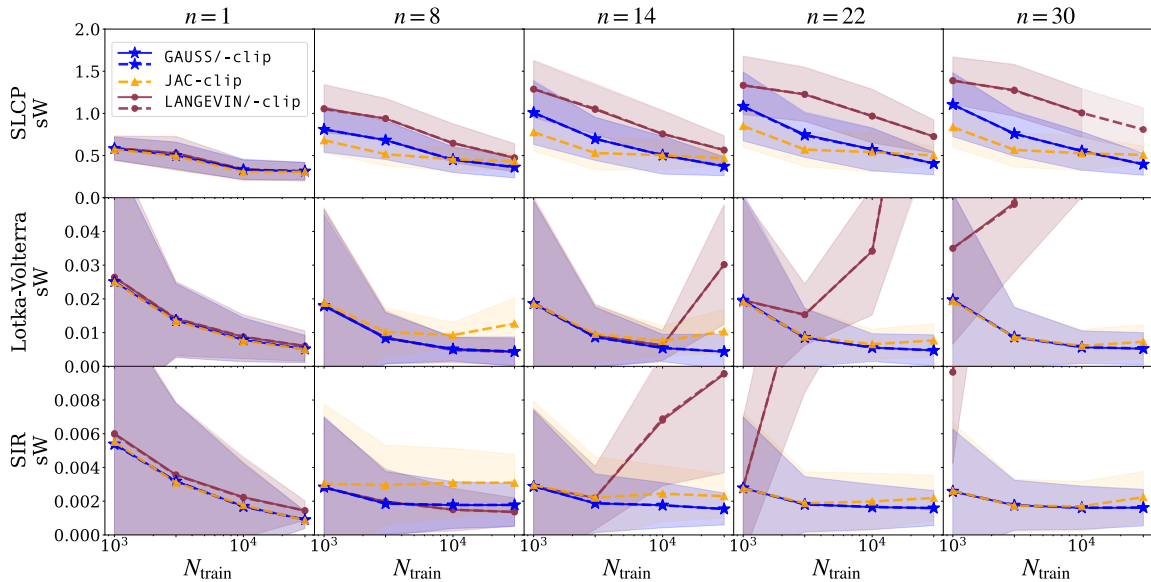


Figure 3: Sliced Wasserstein (sW) distance as a function of $N_{\text{train}} \in [10^3, 3.10^3, 10^4, 3.10^4]$ between the samples obtained by each algorithm (**GAUSS**, **JAC** and **LANGEVIN**) and the true tall posterior distribution $p(\theta \mid x_{1:n}^*)$ for $n \in [1, 8, 14, 22, 30]$. Mean and std over 25 different parameters $\theta^* \sim \lambda(\theta)$.

The used score model is always a MLP with 3 hidden layers, trained on N_{train} samples over 5000 epochs using the Adam optimizer. Further details are provided in Appendix E. According to the *equivalent time setting* defined in Section 4.1, we use 1 000 sampling steps for **GAUSS** and 400 steps for **JAC** and **LANGEVIN**. We also consider *clipped* versions for all proposed algorithms (represented with dashed lines), where we ensure that the samples generated at every step stay within the region of high probability for the standard Gaussian distribution. We introduce this numerical procedure to stabilize the **JAC** and **LANGEVIN** algorithms, that we found to be less robust than **GAUSS**, with quickly diverging sW for poor score estimators; see Section 4.1. Note that this procedure significantly slows down the sampling procedure and can introduce some bias in the posterior approximation.

Our empirical evaluation samples twenty-five⁴ different ground truth parameters $\theta^* \sim \lambda(\theta)$ from the prior distribution, each of which used to simulate observations $x_j^* \sim p(x \mid \theta^*)$ for $j = 1, \dots, n$, later plugged in as conditioning variables in the tall posterior $p(\theta \mid x_{1:n}^*)$. For all three examples, samples from the true tall posterior can be obtained via MCMC using the `numpyro` package (Phan et al., 2019; Bingham et al., 2019) and used to compute the sliced Wasserstein (sW) distance in every setting corresponding to varying N_{train} and n . In Appendix H, we also report results for the Maximum Mean Discrepancy (MMD) and the Classifier-Two-Sample Test (C2ST) metrics from the `sbibm` package.

Figure 3 portrays the sW distance for each task as a function of the size N_{train} of the training set for the score model. Larger values of N_{train} are expected to yield better score estimates and thus more accurate posterior approximations. This is represented by a decreasing tendency towards 0 of the sW. Overall, we observe that **GAUSS** outperforms all other algorithms. It yields consistently lower distance values than

⁴We removed outliers, which correspond to a sW for **GAUSS** above the 99% quantile (or NaN values).

LANGEVIN and scales to high n values, while **LANGEVIN** diverges for $n \geq 14$ for the Lotka–Volterra and SIR examples. Note that **JAC** diverges in every case as soon as $n > 1$, which is why we didn’t include it in the plots. On the other hand, **JAC-clip** is more or less equivalent to **GAUSS**, with slightly better results for SLCP. We refer the reader to Appendix I for results on additional tasks from the SBI benchmark. Here, all samplers fail to accurately infer the tall posterior in more complex data settings, which opens up the question on the scalability the Gaussian approximation. One limitation consists in the multiple score network evaluations, which can lead to an accumulation of errors with increasing n (see Appendix H). As a response, Appendix L.2 includes results of a *partially* factorized version of our method, as proposed by Geffner et al. (2023), allowing the best trade-off between simulation cost and number of network evaluations.

4.3 Inverting a non-linear model from computational neuroscience

We illustrate our proposal on a classic model from computational neuroscience and consider the Bayesian inversion of the Jansen & Rit neural mass model (JRNMM) (Jansen and Rit, 1995). Neural mass models are non-linear models constructed based on physiologically motivated stochastic differential equations and are able to replicate oscillatory electrical signals experimentally observed with electroencephalography (EEG) and are commonly used in large-scale simulators of the brain (Sanz Leon et al., 2013). We follow the setup proposed by Rodrigues et al. (2021). Specifically, we consider a stochastic version of the JRNMM (Ableidinger et al., 2017) with a uniform prior placed over the range of physiologically meaningful values of the simulator parameters and use the code provided by Buckwar et al. (2019). The output $x(t)$ of this generative model is a time series obtained by taking as input a set of four parameters $\theta = (C, \mu, \sigma, g)$. All parameters have a physiological interpretation and we invite the reader to check the above references for a detailed explanation on each one of them. It is worth mentioning, however, that there exists a coupling-effect of parameters g and (μ, σ) on the amplitude of the output signal $x(t)$, meaning that the model is non-identifiable: the same observed signal $x^*(t)$ could be generated with larger (smaller) values of g and smaller (larger) values of μ and σ . This indeterminacy makes the posterior inference problem ill-posed and we show next how a *tall data* posterior can give more precise information on how to invert the simulator.

We estimate the tall data posterior of JRNMM using **GAUSS**, **JAC** and **LANGEVIN**. The posterior score was estimated using a MLP trained on $N_{\text{train}} = 50\,000$ samples from the joint p.d.f. Further details about the architecture and training procedure of the score model can be found in Appendices E and J. The accuracy of each sampling algorithm was assessed using an additional calibration dataset of 10 000 samples with the ℓ -C2ST diagnostic, recently proposed by Linhart et al. (2023) and implemented in the `sbi` toolbox. Results are reported in Appendix J. They show that the p -values obtained for **GAUSS** are always above the significance level set at $\alpha = 0.05$, which means that there is no evidence that the estimated posterior is not statistically consistent with the true tall posterior at $x_{1:n}^*$. This is not the case for **JAC** and **LANGEVIN**, which is why we only report results for **GAUSS** next.

We illustrate the ability of our tall posterior to concentrate around the true parameters θ^* used to simulate the observations $x_{1:n}^*$ as n increases. This is quantified with the MMD between the posterior marginals and the Dirac distribution δ_{θ^*} , computed on 10 000 samples obtained with **GAUSS**. Figure 4 portrays the results for a simplified setting in which the gain parameter is fixed at $g = 0$ so to lift the indeterminacy on (μ, σ) . We observe as expected a progressive concentration around θ^* , with sharper posterior marginals and decreasing MMD. In Appendix J, we include the results obtained for the full (4D) JRNMM for which the tall posterior takes a “sharpened banana” shape: while we observe a concentration around (C, g) , the dispersion along the dimensions of (μ, σ) is sustained.

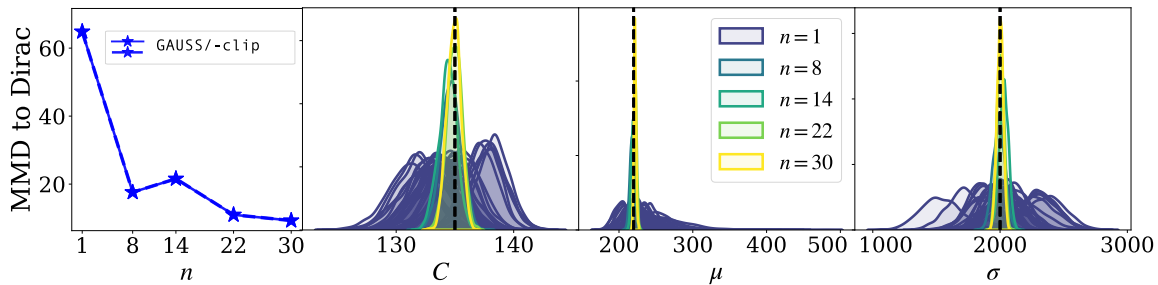


Figure 4: Inference on the 3D JRNMM (fixed $g = 0$) with **GAUSS**. Left: MMD between the marginals of the approximate posterior and the Dirac of the true parameters θ^* (black dashed lines) used to simulate the observations $x_{1:n}^*$. Right: Histograms of the 1D marginals of the inferred posterior samples for 30 single observations x_1^*, \dots, x_{30}^* ($n = 1$) and observation sets $x_{1:n}^*$ of increasing size.

5 Conclusion

The *tall data* setting considered in this paper provides a way of parsing extra observations in an efficient way for SBI. Our method only requires the training of an initial score model amortized for single observations to construct the score of the *tall data* posterior. This allows **GAUSS** and **JAC** to be more simulation efficient, avoiding the shortcomings of the augmented datasets required by NPE. Moreover, we tackle directly the challenge of constructing a diffused version of the posterior distribution for *tall data* based on a second order approximations of the backward diffusion kernels. Further research will investigate the scalability of this approximation both theoretically and practically. Our method benefits from recent advances of score-diffusion literature, such as DDIM (Song et al., 2021b), to perform backward sampling of the diffusion path and obtain samples from the posterior distribution in a much faster and stable way than the annealed Langevin procedure used in Geffner et al. (2023). We have illustrated the performance of our methods on different settings of increasing complexity, considering in particular three examples from the SBI benchmark, and applying our methodology to a challenging non-linear model from computational neuroscience. We demonstrated the superiority of our methods in terms of sample quality for almost all examples, and the reduced computational cost and increased numerical stability in every instance. We expect that our work will encourage other researchers to explore the score-diffusion framework for SBI problems.

Acknowledgements

Julia Linhart is recipient of the Pierre-Aguilar Scholarship and thankful for the funding of the Capital Fund Management (CFM). The work of G. Cardoso was supported by the Investment of the Future Grant, ANR-10-IAHU-04, from the government of France through the Agence National de la Recherche. Alexandre Gramfort thanks the support of the ANR BrAIN (ANR-20-CHIA0016) grant.

Numerical computation was enabled by the scientific Python ecosystem: `numpy` (Harris et al., 2020), `scipy` (Virtanen et al., 2020), `matplotlib` (Hunter, 2007), `seaborn` (Waskom, 2021), and `pytorch` (Paszke et al., 2019).

Impact statement

This paper presents work whose goal is to advance the field of machine learning applied to science. Although we base our approach on deep generative models, for which many ethical and societal questions are of interest, we do not feel that our specific application could generate any concerning issues. It is worth noting that one of our main contributions is the reduction in neural network evaluations for the *tall data* posterior sampling, which can be immediately translated into reduced energy consumption.

References

- Ableidinger, M., Buckwar, E., and Hinterleitner, H. (2017). A stochastic version of the Jansen and Rit neural mass model: Analysis and numerics. *The Journal of Mathematical Neuroscience*, 7(1).
- Bardenet, R., Doucet, A., and Holmes, C. (2015). On Markov chain Monte Carlo methods for tall data. *Journal of Machine Learning Research*, 18:1–43.
- Bhatia, R. (2006). *Positive definite matrices*. Princeton Series in Applied Mathematics. Princeton University Press, Princeton, NJ.
- Bingham, E., Chen, J. P., Jankowiak, M., Obermeyer, F., Pradhan, N., Karaletsos, T., Singh, R., Szerlip, P. A., Horsfall, P., and Goodman, N. D. (2019). PYRO: Deep universal probabilistic programming. *J. Mach. Learn. Res.*, 20:28:1–28:6.
- Boys, B., Girolami, M., Pidstrigach, J., Reich, S., Mosca, A., and Akyildiz, O. D. (2023). Tweedie moment projected diffusions for inverse problems. *arXiv preprint arXiv:2310.06721*.
- Brosse, N., Durmus, A., Moulines, E., and Sabanis, S. (2017). The tamed unadjusted langevin algorithm.
- Buckwar, E., Tamborrino, M., and Tubikanec, I. (2019). Spectral density-based and measure-preserving ABC for partially observed diffusion processes. an illustration on hamiltonian SDEs. *Statistics and Computing*, 30(3):627–648.
- Cranmer, K., Brehmer, J., and Louppe, G. (2020). The frontier of simulation-based inference. *Proceedings of the National Academy of Sciences (PNAS)*, 117:30055–30062.
- Dax, M., Green, S. R., Gair, J., Pürrer, M., Wildberger, J., Macke, J. H., Buonanno, A., and Schölkopf, B. (2023). Neural importance sampling for rapid and reliable gravitational-wave inference. *Phys. Rev. Lett.*, 130:171403.
- Geffner, T., Papamakarios, G., and Mnih, A. (2023). Compositional Score Modeling for Simulation-Based Inference. In Krause, A., Brunskill, E., Cho, K., Engelhardt, B., Sabato, S., and Scarlett, J., editors, *Proceedings of the 40th International Conference on Machine Learning*, volume 202 of *Proceedings of Machine Learning Research*, pages 11098–11116. PMLR.
- Gloeckler, M., Deistler, M., Weilbach, C., Wood, F., and Macke, J. H. (2024). All-in-one simulation-based inference.

- Gonçalves, P. J., Lueckmann, J.-M., Deistler, M., Nonnenmacher, M., Öcal, K., Bassetto, G., Chintaluri, C., Podlaski, W. F., Haddad, S. A., Vogels, T. P., Greenberg, D. S., and Macke, J. H. (2020). Training deep neural density estimators to identify mechanistic models of neural dynamics. *eLife*, 9:e56261.
- Goodfellow, I., Pouget-Abadie, J., Mirza, M., Xu, B., Warde-Farley, D., Ozair, S., Courville, A., and Bengio, Y. (2014). Generative Adversarial Nets. In Ghahramani, Z., Welling, M., Cortes, C., Lawrence, N., and Weinberger, K., editors, *Advances in Neural Information Processing Systems*, volume 27. Curran Associates, Inc.
- Greenberg, D., Nonnenmacher, M., and Macke, J. (2019). Automatic posterior transformation for likelihood-free inference. In Chaudhuri, K. and Salakhutdinov, R., editors, *Proceedings of the 36th International Conference on Machine Learning*, volume 97, pages 2404–2414. PMLR.
- Harris, C. R., Millman, K. J., van der Walt, S. J., Gommers, R., Virtanen, P., Cournapeau, D., Wieser, E., Taylor, J., Berg, S., Smith, N. J., Kern, R., Picus, M., Hoyer, S., van Kerkwijk, M. H., Brett, M., Haldane, A., del Río, J. F., Wiebe, M., Peterson, P., Gérard-Marchant, P., Sheppard, K., Reddy, T., Weckesser, W., Abbasi, H., Gohlke, C., and Oliphant, T. E. (2020). Array programming with NumPy. 585(7825):357–362. Number: 7825 Publisher: Nature Publishing Group.
- Hermans, J., Begy, V., and Louppe, G. (2020). Likelihood-free MCMC with amortized approximate ratio estimators. In III, H. D. and Singh, A., editors, *Proceedings of the 37th International Conference on Machine Learning*, volume 119 of *Proceedings of Machine Learning Research*, pages 4239–4248. PMLR.
- Ho, J., Jain, A., and Abbeel, P. (2020). Denoising diffusion probabilistic models. In Larochelle, H., Ranzato, M., Hadsell, R., Balcan, M., and Lin, H., editors, *Advances in Neural Information Processing Systems*, volume 33, pages 6840–6851.
- Ho, J. and Salimans, T. (2021). Classifier-free diffusion guidance. In *NeurIPS 2021 Workshop on Deep Generative Models and Downstream Applications*.
- Hunter, J. D. (2007). Matplotlib: A 2D graphics environment. 9(3):90–95. Conference Name: Computing in Science & Engineering.
- Hyvärinen, A. and Dayan, P. (2005). Estimation of non-normalized statistical models by score matching. *Journal of Machine Learning Research*, 6(4).
- Jansen, B. H. and Rit, V. G. (1995). Electroencephalogram and visual evoked potential generation in a mathematical model of coupled cortical columns. *Biological Cybernetics 1995* 73:4, 73:357–366.
- Karras, T., Aittala, M., Aila, T., and Laine, S. (2022). Elucidating the design space of diffusion-based generative models. In Koyejo, S., Mohamed, S., Agarwal, A., Belgrave, D., Cho, K., and Oh, A., editors, *Advances in Neural Information Processing Systems*, volume 35, pages 26565–26577.
- Linhart, J., Gramfort, A., and Rodrigues, P. L. C. (2023). L-c2st: Local diagnostics for posterior approximations in simulation-based inference.
- Lueckmann, J.-M., Boelts, J., Greenberg, D., Gonçalves, P., and Macke, J. (2021). Benchmarking simulation-based inference. In Banerjee, A. and Fukumizu, K., editors, *Proceedings of The 24th International Conference on Artificial Intelligence and Statistics*, volume 130 of *Proceedings of Machine Learning Research*, pages 343–351. PMLR.

- Papamakarios, G., Nalisnick, E., Rezende, D. J., Mohamed, S., and Lakshminarayanan, B. (2021). Normalizing flows for probabilistic modeling and inference. *Journal of Machine Learning Research*, 22:1–64.
- Papamakarios, G., Sterratt, D., and Murray, I. (2019). Sequential neural likelihood: Fast likelihood-free inference with autoregressive flows. In Chaudhuri, K. and Sugiyama, M., editors, *Proceedings of the Twenty-Second International Conference on Artificial Intelligence and Statistics*, volume 89 of *Proceedings of Machine Learning Research*, pages 837–848. PMLR.
- Paszke, A., Gross, S., Massa, F., Lerer, A., Bradbury, J., Chanan, G., Killeen, T., Lin, Z., Gimelshein, N., Antiga, L., Desmaison, A., Köpf, A., Yang, E. Z., DeVito, Z., Raison, M., Tejani, A., Chilamkurthy, S., Steiner, B., Fang, L., Bai, J., and Chintala, S. (2019). Pytorch: An imperative style, high-performance deep learning library. *CoRR*, abs/1912.01703.
- Phan, D., Pradhan, N., and Jankowiak, M. (2019). Composable effects for flexible and accelerated probabilistic programming in NumPyro. *arXiv preprint arXiv:1912.11554*.
- Roberts, G. O. and Tweedie, R. L. (1996). Exponential convergence of Langevin distributions and their discrete approximations. *Bernoulli*, pages 341–363.
- Rodrigues, P. L. C., Moreau, T., Louppe, G., and Gramfort, A. (2021). HNPE: Leveraging Global Parameters for Neural Posterior Estimation. In *NeurIPS 2021*, Sydney (Online), Australia.
- Sanz Leon, P., Knock, S., Woodman, M., Domide, L., Mersmann, J., McIntosh, A., and Jirsa, V. (2013). The Virtual Brain: a simulator of primate brain network dynamics. *Frontiers in Neuroinformatics*, 7:10.
- Sharrock, L., Simons, J., Liu, S., and Beaumont, M. (2022). Sequential neural score estimation: Likelihood-free inference with conditional score based diffusion models.
- Song, J., Meng, C., and Ermon, S. (2021a). Denoising diffusion implicit models. In *International Conference on Learning Representations*.
- Song, J., Vahdat, A., Mardani, M., and Kautz, J. (2023). Pseudoinverse-guided diffusion models for inverse problems. In *International Conference on Learning Representations*.
- Song, Y. and Ermon, S. (2019). Generative modeling by estimating gradients of the data distribution. In Wallach, H., Larochelle, H., Beygelzimer, A., d'Alché-Buc, F., Fox, E., and Garnett, R., editors, *Advances in Neural Information Processing Systems*, volume 32. Curran Associates, Inc.
- Song, Y., Sohl-Dickstein, J., Kingma, D. P., Kumar, A., Ermon, S., and Poole, B. (2021b). Score-based generative modeling through stochastic differential equations. In *International Conference on Learning Representations*.
- Vincent, P. (2011). A connection between score matching and denoising autoencoders. *Neural computation*, 23(7):1661–1674.
- Virtanen, P., Gommers, R., Oliphant, T. E., Haberland, M., Reddy, T., Cournapeau, D., Burovski, E., Peterson, P., Weckesser, W., Bright, J., van der Walt, S. J., Brett, M., Wilson, J., Millman, K. J., Mayorov, N., Nelson, A. R. J., Jones, E., Kern, R., Larson, E., Carey, C. J., Polat, I., Feng, Y., Moore, E. W., VanderPlas, J., Laxalde, D., Perktold, J., Cimrman, R., Henriksen, I., Quintero, E. A., Harris, C. R., Archibald, A. M., Ribeiro, A. H., Pedregosa, F., and van Mulbregt, P. (2020). *scipy 1.0: fundamental algorithms for scientific computing in python*. 17(3):261–272. Number: 3 Publisher: Nature Publishing Group.

Waskom, M. L. (2021). *seaborn: statistical data visualization*. 6(60):3021.

Yang, L., Zhang, Z., Song, Y., Hong, S., Xu, R., Zhao, Y., Zhang, W., Cui, B., and Yang, M.-H. (2023). Diffusion models: A comprehensive survey of methods and applications. *ACM Computing Surveys*, 56(4):1–39.

Zaheer, M., Kottur, S., Ravanbakhsh, S., Póczos, B., Salakhutdinov, R. R., and Smola, A. J. (2017). Deep sets. In Guyon, I., Luxburg, U. V., Bengio, S., Wallach, H., Fergus, R., Vishwanathan, S., and Garnett, R., editors, *Advances in Neural Information Processing Systems*, volume 30. Curran Associates, Inc.

A Proofs

A.1 Proof of Lemma 3.1

Let $(\mu_k)_{1 \leq k \leq K} \in (\mathbb{R}^m)^K$ and $(\Sigma_k)_{1 \leq k \leq K}$ be covariance matrices in $\mathbb{R}^{m \times m}$. Denote by p_k the Gaussian pdf with mean μ_k and covariance matrix Σ_k . Note that

$$p_k : \theta_0 \mapsto \exp \left(\tilde{\zeta}_k + (\Sigma_k^{-1} \mu_k)^\top \theta_0 - \frac{1}{2} \theta_0^\top \Sigma_k^{-1} \theta_0 \right),$$

where

$$\tilde{\zeta}_k = -\frac{1}{2} (m \log 2\pi - \log |\Sigma_k^{-1}| + \mu_k^\top \Sigma_k^{-1} \mu_k).$$

Therefore,

$$\begin{aligned} \prod_{k=1}^K p_k(\theta_0) &= \exp \left(\sum_{k=1}^K \tilde{\zeta}_k - \tilde{\zeta}_{\text{all}} \right) \exp \left(\tilde{\zeta}_{\text{all}} + \tilde{\eta}^\top \theta_0 - \frac{1}{2} \theta_0^\top \tilde{\Lambda} \theta_0 \right) \\ &= \exp \left(\sum_{k=1}^K \tilde{\zeta}_k - \tilde{\zeta}_{\text{all}} \right) \mathcal{N}(\theta_0; \tilde{\Lambda}^{-1} \tilde{\eta}, \tilde{\Lambda}^{-1}), \end{aligned}$$

with $\tilde{\eta} = \sum_{k=1}^K \Sigma_k^{-1} \mu_k$, $\tilde{\Lambda} = \sum_{k=1}^K \Sigma_k^{-1}$, and $\tilde{\zeta}_{\text{all}} = -(m \log 2\pi - \log |\tilde{\Lambda}| + \tilde{\eta}^\top \tilde{\Lambda}^{-1} \tilde{\eta})/2$. We can apply this result to equation (10) with

$$\begin{aligned} \eta(\theta) &= \sum_{j=1}^n \Sigma_t^{-1}(\theta, x_j) \mu_t(\theta, x_j) + (1-n) \Sigma_{t,\lambda}^{-1}(\theta) \mu_{t,\lambda}(\theta), \\ \Lambda(\theta) &= \sum_{j=1}^n \Sigma_t^{-1}(\theta, x_j) + (1-n) \Sigma_{t,\lambda}^{-1}(\theta), \end{aligned}$$

since by assumption $\Lambda(\theta)$ is definite positive. This provides the following reformulation of equation (10), which concludes the proof:

$$\ell_\lambda(\theta, x_{1:n}^*) = \log \int \exp \left(\sum_{j=1}^n \zeta_j(\theta) + (1-n) \zeta_\lambda(\theta) - \zeta_{\text{all}}(\theta) \right) \mathcal{N}(\theta_0; \Lambda^{-1}(\theta) \eta(\theta), \Lambda^{-1}(\theta)) d\theta_0.$$

A.2 Proof of Lemma 3.2

Let $\zeta(\mu, \Sigma^{-1}) = -(m \log 2\pi - \log |\Sigma^{-1}| + \mu^\top \Sigma^{-1} \mu) / 2$. Then

$$\begin{aligned} \nabla_\theta \zeta_j(\theta, x_j) &= \nabla_\theta \zeta(\mu_{t,j}(\theta), \Sigma_{t,j}^{-1}(\theta)) \\ &= \nabla_\mu \zeta(\mu_{t,j}(\theta), \Sigma_{t,j}^{-1}(\theta))^\top \nabla_\theta \mu_{t,j}(\theta) + \nabla_{\Sigma^{-1}} \zeta(\mu_{t,j}(\theta), \Sigma_{t,j}^{-1}(\theta)) \nabla_\theta \Sigma_{t,j}^{-1}(\theta), \end{aligned}$$

where

$$\nabla_\mu \zeta(\mu, \Sigma^{-1}) = -\Sigma^{-1} \mu \quad \text{and} \quad \nabla_{\Sigma^{-1}} \zeta(\mu, \Sigma^{-1}) = (1/2) (\Sigma - \mu \mu^\top).$$

Therefore, we obtain

$$\begin{aligned}\nabla_{\theta}\zeta_j(\theta, x_j) &= -\mu_{t,j}(\theta)^\top \Sigma_{t,j}^{-1}(\theta)^\top \nabla_{\theta}\mu_{t,j}(\theta) \\ &\quad + (1/2) (\Sigma_{t,j}(\theta) - \mu_{t,j}(\theta)\mu_{t,j}(\theta)^\top) \nabla_{\theta}\Sigma_{t,j}^{-1}(\theta).\end{aligned}$$

Note that $\nabla_{\theta}\mu_{t,j}(\theta) = (\sqrt{\alpha_t}/v_t)\Sigma_{t,j}(\theta)$, which leads to

$$\begin{aligned}\nabla_{\theta}\zeta_j(\theta, x_j) &= -\frac{\sqrt{\alpha_t}}{v_t}\mu_{t,j}(\theta) + (1/2) (\Sigma_{t,j}(\theta) - \mu_{t,j}(\theta)\mu_{t,j}(\theta)^\top) \nabla_{\theta}\Sigma_{t,j}^{-1}(\theta) \\ &= -v_t^{-1}\theta - \nabla_{\theta}\log p_t(\theta)x_j + (1/2) (\Sigma_{t,j}(\theta) - \mu_{t,j}(\theta)\mu_{t,j}(\theta)^\top) \nabla_{\theta}\Sigma_{t,j}^{-1}(\theta).\end{aligned}$$

This leads to

$$\begin{aligned}\nabla_{\theta}\ell_{\lambda}(\theta, x_{1:n}) &= -(1-n)\nabla_{\theta}\log p_t^{\lambda}(\theta) - \sum_{j=1}^n \nabla_{\theta}\log p_t(\theta)x_j^* - v_t^{-1}\theta - \nabla_{\theta}\zeta_{\text{all}}(\theta) \\ &\quad + (1/2) \left[\sum_{j=1}^n (\Sigma_{t,j}(\theta) - \mu_{t,j}(\theta)\mu_{t,j}(\theta)^\top) \nabla_{\theta}\Sigma_{t,j}^{-1}(\theta) \right] \\ &\quad + \frac{1-n}{2} (\Sigma_{t,\lambda}(\theta) - \mu_{t,\lambda}(\theta)\mu_{t,\lambda}(\theta)^\top) \nabla_{\theta}\Sigma_{t,\lambda}^{-1}(\theta, x_j).\end{aligned}$$

The score is then given by

$$\begin{aligned}\nabla_{\theta}\log p_t(\theta)x_{1:n} &= -v_t^{-1}\theta - \nabla_{\theta}\zeta_{\text{all}}(\theta) \\ &\quad + (1/2) \left[\sum_{j=1}^n (\Sigma_{t,j}(\theta) - \mu_{t,j}(\theta)\mu_{t,j}(\theta)^\top) \nabla_{\theta}\Sigma_{t,j}^{-1}(\theta) \right] \\ &\quad + \frac{1-n}{2} (\Sigma_{t,\lambda}(\theta) - \mu_{t,\lambda}(\theta)\mu_{t,\lambda}(\theta)^\top) \nabla_{\theta}\Sigma_{t,\lambda}^{-1}(\theta, x_j).\end{aligned}$$

We now estimate $\nabla_{\theta}\zeta_{\text{all}}(\theta)$ by noting that $\zeta_{\text{all}} = \zeta(\Lambda(\theta)^{-1}\eta(\theta), \Lambda(\theta))$. We obtain

$$\begin{aligned}\nabla_{\theta}\zeta_{\text{all}}(\theta) &= -\nabla_{\theta}(\Lambda(\theta)^{-1}\eta(\theta))\eta(\theta) + (1/2) [\mathbf{I}_m - \Lambda(\theta)^{-1}\eta(\theta)\eta(\theta)^\top] \Lambda(\theta)^{-1}\nabla_{\theta}\Lambda(\theta) \\ &= -\Lambda(\theta)^{-1}\nabla_{\theta}\eta(\theta)\eta(\theta) - \eta(\theta)^\top \nabla\Lambda(\theta)^{-1}\eta(\theta) + (1/2) [\mathbf{I}_m - \Lambda(\theta)^{-1}\eta(\theta)\eta(\theta)^\top] \Lambda(\theta)^{-1}\nabla_{\theta}\Lambda(\theta).\end{aligned}$$

Note now that

$$\begin{aligned}\nabla_{\theta}\eta(\theta) &= \sum_{j=1}^n \Sigma_{t,j}^{-1}(\theta)\nabla_{\theta}\mu_{t,j}(\theta) + \mu_{t,j}(\theta)^\top \nabla_{\theta}\Sigma_{t,j}^{-1}(\theta) \\ &\quad + (1-n) (\Sigma_{t,\lambda}^{-1}(\theta)\nabla_{\theta}\mu_{t,\lambda}(\theta) + \mu_{t,\lambda}(\theta)^\top \nabla_{\theta}\Sigma_{t,\lambda}^{-1}(\theta)) \\ &= \frac{\sqrt{\alpha_t}}{v_t}\mathbf{I}_m + \sum_{j=1}^n \mu_{t,j}(\theta)^\top \nabla_{\theta}\Sigma_{t,j}^{-1}(\theta) + (1-n)\mu_{t,\lambda}(\theta)^\top \nabla_{\theta}\Sigma_{t,\lambda}^{-1}(\theta),\end{aligned}$$

which leads to

$$\nabla_{\theta}\eta(\theta)\eta(\theta) = \frac{\sqrt{\alpha_t}}{v_t}\eta(\theta) + \left[\sum_{j=1}^n \mu_{t,j}(\theta)^\top \nabla_{\theta}\Sigma_{t,j}^{-1}(\theta) + (1-n)\mu_{t,\lambda}(\theta)^\top \nabla_{\theta}\Sigma_{t,\lambda}^{-1}(\theta) \right] \eta(\theta). \quad (13)$$

Note that

$$\begin{aligned}\sqrt{\alpha_t}\eta(\theta) &= \sum_{j=1}^n \Sigma_{t,j}^{-1}(\theta) (\theta + v_t \nabla_{\theta} \log p_t(\theta) x_j) + (1-n)\Sigma_{t,\lambda}^{-1}(\theta) (\theta + v_t \nabla_{\theta} \log p_t^{\lambda}(\theta)) \\ &= \Lambda(\theta)\theta + v_t \left[\sum_{j=1}^n \Sigma_{t,j}^{-1}(\theta) \nabla_{\theta} \log p_t(\theta) x_j + (1-n)\Sigma_{t,\lambda}^{-1}(\theta) \nabla_{\theta} \log p_t^{\lambda}(\theta) \right],\end{aligned}$$

which finally leads to

$$\nabla_{\theta} \log p_t(\theta | x_{1:n}^*) = \Lambda(\theta)^{-1} \left[\sum_{j=1}^n \Sigma_{t,j}^{-1}(\theta) \nabla_{\theta} \log p_t(\theta) x_j + (1-n)\Sigma_{t,\lambda}^{-1}(\theta) \nabla_{\theta} \log p_t^{\lambda}(\theta) \right] + F(\theta, x_{1:n}^*),$$

where

$$\begin{aligned}F(\theta, x_{1:n}^*) &= \eta(\theta)^{\top} \nabla \Lambda(\theta)^{-1} \eta(\theta) + (1/2) [\mathbf{I}_m - \Lambda(\theta)^{-1} \eta(\theta) \eta(\theta)^{\top}] \Lambda(\theta)^{-1} \nabla_{\theta} \Lambda(\theta) \\ &\quad + (1/2) \left[\sum_{j=1}^n (\Sigma_{t,j}(\theta) - \mu_{t,j}(\theta) \mu_{t,j}(\theta)^{\top}) \nabla_{\theta} \Sigma_{t,j}^{-1}(\theta) \right] \\ &\quad + \frac{1-n}{2} (\Sigma_{t,\lambda}(\theta) - \mu_{t,\lambda}(\theta) \mu_{t,\lambda}(\theta)^{\top}) \nabla_{\theta} \Sigma_{t,\lambda}^{-1}(\theta, x_j).\end{aligned}$$

B Positive Definiteness of $\Lambda(\theta)$

The approximation described in Section 3.2 is only valid if matrix $\Lambda(\theta)$ is symmetric positive definite (SPD), i.e. it is a valid covariance matrix. In what follows, we will show what are the conditions on the choice of the p.d.f. for the prior distribution that will ensure such property. Using the partial ordering defined by the convex cone of SPD matrices (Bhatia, 2006) it follows that:

$$\Lambda(\theta) \succ 0 \iff \sum_{j=1}^n \Sigma_t^{-1}(\theta, x_j) + (1-n)\Sigma_{t,\lambda}^{-1}(\theta) \succ 0, \quad (14)$$

$$\iff \sum_{j=1}^n \Sigma_t^{-1}(\theta, x_j) \succ (n-1)\Sigma_{t,\lambda}^{-1}(\theta), \quad (15)$$

$$\iff \Sigma_{t,\lambda}(\theta) \succ \left(\frac{1}{(n-1)} \sum_{j=1}^n \Sigma_t^{-1}(\theta, x_j) \right)^{-1}. \quad (16)$$

Note that as n increases, the R.H.S. of the inequality converges to the harmonic mean of the $\Sigma_t(\theta, x_j)$, which helps building an intuition to the correct choice for the covariance $\Sigma_{t,\lambda}(\theta)$ of the prior. For instance, a sufficient choice (not necessarily optimal) would be to have a $\Sigma_{t,\lambda}(\theta)$ whose associated ellipsoid⁵ covers the ellipsoids generated by all other covariance matrices $\Sigma_t(\theta, x_j)$.

⁵The ellipsoid \mathcal{E}_A associated with SPD matrix A is defined as $\mathcal{E}_A = \{\mathbf{x} : \mathbf{x}^\top A^{-1} \mathbf{x} < 1\}$

C Influence of the correction term $\nabla_{\theta} \ell_{\lambda}(\theta, x_{1:n}^*)$.

Intuition following the definition of the backward kernels in equation (8):

- For $t \rightarrow 1$: the forward kernel and the diffused data distribution approach the noise distribution: $p_t(\theta | x) \xrightarrow{t \rightarrow 1} \mathcal{N}(\theta; 0, \mathbf{I}_m)$ and $q_{t|0}(\theta | \theta_0) \xrightarrow{t \rightarrow 1} \mathcal{N}(\theta; 0, \mathbf{I}_m)$. The backward kernel is thus equivalent to the target data distribution:

$$p_{0|t}(\theta_0 | \theta, x) = \frac{p(\theta_0 | x) q_{t|0}(\theta | \theta_0)}{p_t(\theta | x)} \underset{t \rightarrow 1}{\sim} p(\theta_0 | x). \quad (17)$$

Therefore the backward kernels vary very little with θ , and because they define $\ell_{\lambda}(\theta, x_{1:n}^*)$ (see eq. (10)), its gradient is close to zero. In other words, $\nabla_{\theta} \ell_{\lambda}(\theta, x_{1:n}^*)$ has no significant impact at the beginning of the backward diffusion (aka. sampling or generative process).

- For $t \rightarrow 0$: the denominator is the diffused distribution that gets close to the target data distribution $p_t(\theta | x) \xrightarrow{t \rightarrow 0} p(\theta_0 | x)$. Therefore the backward kernel is approximately

$$p_{0|t}(\theta_0 | \theta, x) = \frac{p(\theta_0 | x) q_{t|0}(\theta | \theta_0)}{p_t(\theta | x)} \underset{t \rightarrow 0}{\sim} q_{t|0}(\theta | \theta_0) \xrightarrow{t \rightarrow 0} \delta_{\theta_0}(\theta). \quad (18)$$

Here, the dependence on θ is convergence to a Dirac function. This means that the gradient of $\ell_{\lambda}(\theta, x_{1:n}^*)$ will increase during the sampling process and finally explode when t approaches 0. The correction term therefore plays an important role as we approach the target tall data posterior distribution, at the end of the sampling process.

D Analytical formulas for score and related quantities

D.1 Gaussian case

The considered Bayesian Inference task is to estimate the mean $\theta \in \mathbb{R}^m$ of a Gaussian simulator model $p(x | \theta) = \mathcal{N}(x; \theta, \Sigma)$, given a Gaussian prior $\lambda(\theta) = \mathcal{N}(\theta; \mu_\lambda, \Sigma_\lambda)$. For a single observation x^* , the true posterior is also a Gaussian obtained using Bayes formula, as the product of two Gaussian distributions:

$$p(\theta | x^*) = \mathcal{N}(\theta; \mu_{\text{post}}(x^*), \Sigma_{\text{post}}) \quad (19)$$

with $\mu_{\text{post}}(x^*) = \Sigma_{\text{post}}(\Sigma^{-1}x^* + \Sigma_\lambda^{-1}\mu_\lambda)$ and $\Sigma_{\text{post}} = (\Sigma^{-1} + \Sigma_\lambda^{-1})^{-1}$. Note that in this case, the full posterior can be written as

$$p(\theta | x_{1:n}^*) = \mathcal{N}(\theta; \mu_{\text{post}}(x_{1:n}^*), \Sigma_{\text{post},n}) \quad (20)$$

with $\Sigma_{\text{post},n} = (n\Sigma^{-1} + \Sigma_\lambda^{-1})^{-1}$ and $\mu_{\text{post}}(x_{1:n}^*) = \Sigma_{\text{post},n}(\sum_{j=1}^n \Sigma^{-1}x_j^* + \Sigma_\lambda^{-1}\mu_\lambda)$.

Assume that $q_{t|0}(\theta | \theta_0) = \mathcal{N}(\theta; \sqrt{\alpha_t}\theta_0, v_t\mathbf{I}_m)$; see Section 2. Using standard results (e.g. equation 2.115 in Bishop, 2006), we can derive the analytic formula of the diffused prior

$$p_t^\lambda(\theta) = \int \lambda(\theta_0)q_{t|0}(\theta | \theta_0)d\theta_0 \quad (21)$$

$$= \mathcal{N}(\theta; \sqrt{\alpha_t}\mu_\lambda, \alpha_t\Sigma_\lambda + v_t\mathbf{I}_m) \quad (22)$$

and of the diffused posterior

$$p_t(\theta | x^*) = \int p(\theta_0 | x^*)q_{t|0}(\theta | \theta_0)d\theta_0 \quad (23)$$

$$= \mathcal{N}(\theta; \sqrt{\alpha_t}\mu_{\text{post}}(x^*), \alpha_t\Sigma_{\text{post}} + v_t\mathbf{I}_m). \quad (24)$$

The corresponding Fisher scores are

$$\nabla_\theta \log p_t^\lambda(\theta) = -(\alpha_t\Sigma_\lambda + v_t\mathbf{I}_m)^{-1}(\theta - \sqrt{\alpha_t}\mu_\lambda), \quad (25)$$

$$\nabla_\theta \log p_t(\theta | x^*) = -(\alpha_t\Sigma_{\text{post}} + v_t\mathbf{I}_m)^{-1}(\theta - \sqrt{\alpha_t}\mu_{\text{post}}(x^*)). \quad (26)$$

Replacing the score from (26) in the formulas from (Boys et al., 2023), we get the following expressions for the mean and covariance matrix of the backward diffusion kernel $p_{0|t}(\theta_0 | \theta, x)$:

$$\begin{aligned} \Sigma_t(\theta, x^*) &= \frac{v_t}{\alpha_t} \left(1 - v_t \left(\alpha_t \Sigma_{\text{post}} + v_t \mathbf{I}_m \right)^{-1} \right) = \Sigma_t, \\ \mu_t(\theta, x^*) &= \frac{1}{\sqrt{\alpha_t}} \left(1 - v_t \left(\alpha_t \Sigma_{\text{post}} + v_t \mathbf{I}_m \right)^{-1} \right) \theta + v_t \left(\alpha_t \Sigma_{\text{post}} + v_t \mathbf{I}_m \right)^{-1} \mu_{\text{post}}(x^*) \\ &= \frac{\sqrt{\alpha_t}}{v_t} \Sigma_t \theta + v_t \left(\alpha_t \Sigma_{\text{post}} + v_t \mathbf{I}_m \right)^{-1} \mu_{\text{post}}(x^*). \end{aligned}$$

The same goes for the prior backward diffusion kernel $p_{0|t}^\lambda(\theta_0 | \theta)$:

$$\begin{aligned}\Sigma_{t,\lambda}(\theta) &= \frac{v_t}{\alpha_t} \left(1 - v_t \left(\alpha_t \Sigma_\lambda + v_t \mathbf{I}_m \right)^{-1} \right) = \Sigma_{t,\lambda}, \\ \mu_{t,\lambda}(\theta) &= \frac{1}{\sqrt{\alpha_t}} \left(1 - v_t \left(\alpha_t \Sigma_\lambda + v_t \mathbf{I}_m \right)^{-1} \right) \theta + v_t \left(\alpha_t \Sigma_\lambda + v_t \mathbf{I}_m \right)^{-1} \mu_\lambda \\ &= \frac{\sqrt{\alpha_t}}{v_t} \Sigma_{t,\lambda} \theta + v_t \left(\alpha_t \Sigma_\lambda + v_t \mathbf{I}_m \right)^{-1} \mu_\lambda.\end{aligned}$$

D.2 Score of the diffused Log-Normal prior

The Log-Normal distribution can easily be transformed into a Gaussian distribution:

$$\theta \sim \text{LogNormal}(m, s) \Rightarrow \log \theta \sim \mathcal{N}(m, s).$$

We can therefore directly apply the Gaussian case from the previous section, after transforming the data into the log-space.

D.3 Score of the diffused Uniform prior

Consider the case where the prior is a Uniform distribution $\lambda(\theta) = \mathcal{U}(\theta; a, b)$, with $(a, b) \in \mathbb{R}^m \times \mathbb{R}^m$, the lower and upper bounds respectively. Assume that $q_{t|0}(\theta | \theta_0) = \mathcal{N}(\theta; \sqrt{\alpha_t} \theta_0, v_t \mathbf{I}_m)$; see Section 2 with $v_t = 1 - \alpha_t$. We then get the following analytic formula for the diffused prior:

$$p_t^\lambda(\theta) = \int \lambda(\theta_0) q_{t|0}(\theta | \theta_0) d\theta_0 \quad (27)$$

$$= \frac{1}{\prod_{i=1}^m (b_i - a_i)} \int_{[a_1, b_1] \times \dots \times [a_m, b_m]} \mathcal{N}(\theta; \sqrt{\alpha_t} \theta_0, v_t \mathbf{I}_m) \quad (28)$$

$$= \frac{1}{\sqrt{\alpha_t} \prod_{i=1}^m (b_i - a_i)} \prod_{i=1}^m (\Phi(\sqrt{\alpha_t} b_i; \theta_i, v_t) - \Phi(\sqrt{\alpha_t} a_i; \theta_i, v_t)), \quad (29)$$

where $\Phi(\cdot; \mu, \sigma^2)$ is the c.d.f. of a univariate Gaussian with mean μ and variance σ^2 . The score of the above quantity is then simply obtained by computing the score of each one-dimensional element in the above product. For $i \in [1, m]$, $\nabla_\theta \log p_t^\lambda(\theta)_i = \nabla_{\theta_i} \log f(\theta_i) = \frac{\nabla_{\theta_i} f(\theta_i)}{f(\theta_i)}$ with

$$f(\theta_i) = (\Phi(\sqrt{\alpha_t} b_i; \theta_i, v_t) - \Phi(\sqrt{\alpha_t} a_i; \theta_i, v_t)) \quad (30)$$

$$\nabla_{\theta_i} f(\theta_i) = -\frac{1}{\sqrt{\alpha_t} v_t} (\mathcal{N}(\sqrt{\alpha_t} b_i; \theta_i, v_t) - \mathcal{N}(\sqrt{\alpha_t} a_i; \theta_i, v_t)). \quad (31)$$

D.4 Mixture of Gaussians

In the case of the Mixture of Gaussians, the prior is $\lambda = \mathcal{N}(0, \mathbf{I}_m)$, the simulator is given by $p(x|\theta) = (1/2)\mathcal{N}(x; \theta, \Sigma_1) + (1/2)\mathcal{N}(x; \theta, 1/9\Sigma_2)$ where $\Sigma_1 = 2.25\Sigma$, $\Sigma_2 = 1/9\Sigma$ and Σ is a diagonal matrix with values increasing linearly between 0.6 and 1.4. In this case, the posterior pdf is

$$p(\theta|x) = \omega_1(x)\mathcal{N}(\theta; \mu_1, \Sigma_{1,p}) + \omega_2(x)\mathcal{N}(\theta; \mu_2, \Sigma_{2,p}) \quad (32)$$

where for $i = 1, 2$, $\Sigma_{i,p} = (\Sigma_i^{-1} + \mathbf{I}_m)^{-1}$, $\mu_i = \Sigma_{i,p}\Sigma_i^{-1}x$, $\tilde{\omega}_i(x) = \mathcal{N}(x; \theta, \Sigma_i + \mathbf{I}_m)$ and $\omega_i = \tilde{\omega}_i / \sum_{j=1}^2 \tilde{\omega}_j$.

Therefore, the diffused marginals are

$$p_t(\theta|x) = \omega_1(x)\mathcal{N}(\theta; \alpha_t^{1/2}\mu_1, \alpha_t\Sigma_{1,p} + (1 - \alpha_t)\mathbf{I}_m) + \omega_2(x)\mathcal{N}(\theta; \alpha_t^{1/2}\mu_2, \alpha_t\Sigma_{2,p} + (1 - \alpha_t)\mathbf{I}_m), \quad (33)$$

from which the score is

$$\nabla_{\theta} \log p_t(\theta|x) = -\omega_1(x)(\alpha_t\Sigma_{1,p} + (1 - \alpha_t)\mathbf{I}_m)^{-1}(\theta - \alpha_t^{1/2}\mu_1) - \omega_2(x)(\alpha_t\Sigma_{2,p} + (1 - \alpha_t)\mathbf{I}_m)^{-1}(\theta - \alpha_t^{1/2}\mu_2). \quad (34)$$

E Implementation details

All experiments are implemented with Python combined with PyTorch.

The score network. The same score model architecture and training hyper parameters are used for all tasks. Our implementation of the score model $s_\phi(\theta, x, t)$ is an MLP with layer normalization and 3 hidden layers of 256 hidden features. It takes as input the variables (θ, x, t) and outputs a vector of the same size as $\theta \in \mathbb{R}^m$. Before being passed to the score network, a positional embedding is computed for $t \in [0, 1]$ as per: $(\cos(ti\pi), \sin(ti\pi))_{1 \leq i \leq F}$, where we chose $F = 3$ for the number of frequencies. Optionally, θ and x can each be passed to an embedding network. Note that for the benchmark experiment in Section 4.2, no embedding networks were used, as we chose to use the same score model architecture across all tasks, each with different data dimensions. For the more complex neuroscience application in Section 4.3, θ and x were each embedded with with a MLP with 3 hidden layers of 64 hidden features and output embedding dimension of 32.

The score model is trained by minimizing the denoising score-matching (DSM) loss $\mathbb{E} [\|s_\phi(\theta, x, t) - \nabla_\theta \log q_{t|0}(\theta | \theta_0)\|^2]$, parametrized with the VP-SDE and a linear noise schedule $\beta(t) = 32t$ (Song et al., 2021b). For more stability we actually learn the *noise distribution* ϵ_ϕ (Ho et al., 2020; Song et al., 2021a), which is related to the score function via $\epsilon_\phi(\theta, x, t) = -\sigma(t)s_\phi(\theta, x, t)$. Given a training dataset $(\{(\theta_{0,i}, x_i)\}_{i=1}^{N_s} \sim p(\theta, x), t_i \sim \mathcal{U}(0, 1), z_i \sim \mathcal{N}(0, \mathbf{I}_m)$), the empirical loss function writes:

$$\mathcal{L}(\phi) = \frac{1}{N_s} \sum_{i=1}^{N_s} \|\epsilon_\phi(\theta_i, x_i, t_i) - z_i\|^2, \quad \text{with } \theta_i = \sqrt{\alpha(t_i)}\theta_{0,i} + \sigma(t_i)z_i. \quad (35)$$

Training is done using the Adam optimizer over 5 000 epochs and early stopping using 20% of the training data. Note that early stopping requires to be done with care, since the loss function is stochastic. For each example and training set N_{train} , we therefore trained several models for different learning rates and batch sizes, and selected the one that corresponds to the best trade-off between smallest validation loss and latest stopping epoch (we want the score network to be trained over as many epochs as possible). See Figure 5 that displays the train and validation losses for all SBI examples and explains our model selection strategy (i.e. choices of learning rate and batch size).

The training dataset is always normalized to zero mean and standard variance (for variables θ and x). The same transformation has to be applied to the observations $x_{1:n}^*$ and the prior score function $\nabla_\theta \log p_t^\lambda(\theta)$ during sampling. After sampling, the inverse transformation is applied to the obtained samples, which are then compared to samples from the true posterior distribution $p(\theta | x_{1:n}^*)$. For the cases where the prior and / or the simulator corresponds to a Log-Normal distribution, an additional log-transformation is applied to θ and / or x .⁶

(Diffusion) Posterior Sampling. For sampling the approximate tall posteriors, we use the score-based samplers chosen in Section 4.1 according to the *equivalent time setting*, i.e. DDIM with respectively 1 000 steps, $\eta = 1$ and 400 steps, $\eta = 0.8$ for GAUSS and JAC, and 400 steps for LANGEVIN with the the same hyper-parameters as in (Geffner et al., 2023).

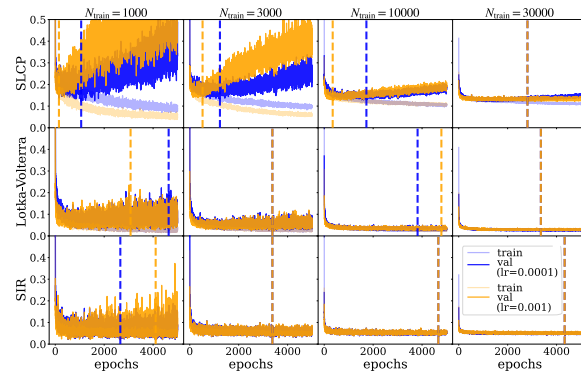
⁶This applies to the prior for both, the Lotka Volterra and SIR examples, and to the simulator for Lotka Volterra only.

The true posterior samples are obtained via MCMC using `numpyro` with `jax`, except for the Gaussian Mixture Toy Model from section 4.1, for which we consider the Metropolis-Adjusted Langevin Algorithm; see (Roberts and Tweedie, 1996). For a given number of observations n , we initialize the samples at $n^{-1} \sum_{j=1}^n x_j^* + \epsilon$ where $\epsilon \sim \mathcal{N}(0, \mathbf{I}_m)$. We run the MALA algorithm for 10^3 iterations with a learning rate of $n^{-1}10^{-3}$. We adapt the learning rate in the first 500 iterations to target an acceptance ratio of 0.5. To do so, we increase the learning rate by a factor of 1.01 if the acceptance rate is larger than 0.5 or by a factor of 0.99 if the acceptance rate is smaller than 0.45.

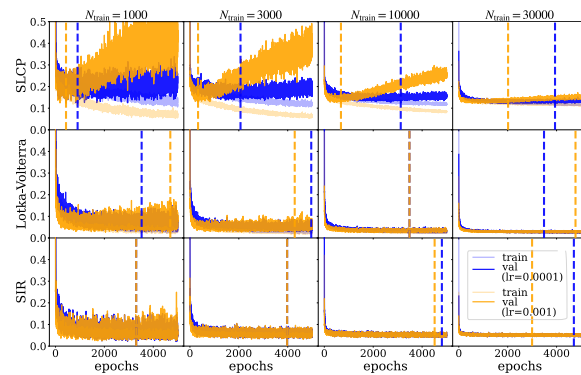
Evaluation metrics. To evaluate the accuracy of the sampling algorithms on the SBI benchmark examples, we compute the distance between 10 000 samples of the true and estimated posterior using three different metrics: the sliced Wasserstein (sW) distance from the `POT` python package with 1 000 projections, the Maximum Mean Discrepancy (MMD) and the Classifier-Two-Sample Test (C2ST), both from the `sbibm` package, with default parameters. For the Jansen and Rit Neural Mass Model, our *real* SBI example from computational neuroscience, no samples from the true posterior are available and the above metrics cannot be computed. We therefore use the *local* Classifier-Two-Sample Test (ℓ -C2ST) recently proposed by Linhart et al. (2023), as implemented in the `sbi` toolbox, with default parameters.

Code and compute resources. The code and guidelines to reproduce all numerical experiments is provided in the following github repository: <https://github.com/JuliaLinhart/diffusions-for-sbi>. This includes specific information about the code environment and installation requirements, mentioned in the "readme.md" file. In this url, we also provide pre-generated data and pre-computed results that are necessary to quickly generate all figures of the paper without extensive computation time.

F Loss functions, training strategy and model selection



(a) Batch size 64.



(b) Batch size 256.

Figure 5: Train and validation losses for the SBI benchmark examples obtained for score networks trained over 5 000 epochs with the Adam optimizer and learning rates $lr = 1e^{-3}$ (orange) and $lr = 1e^{-4}$ (blue). The two Figures respectively corresponds to a batch size of 64 and 256. For small N_{train} , over fitting behavior can be detected (SLCP and Lotka Volterra). In these cases, a higher batch size of 256 is chosen, since it yields more stable loss functions, with delayed over fitting and thus also delayed early stopping. Since the best validation loss in each setting is similar (with small variations due to the stochasticity of the loss function), the learning rate can then be chosen to correspond to the latest early stopping epoch.

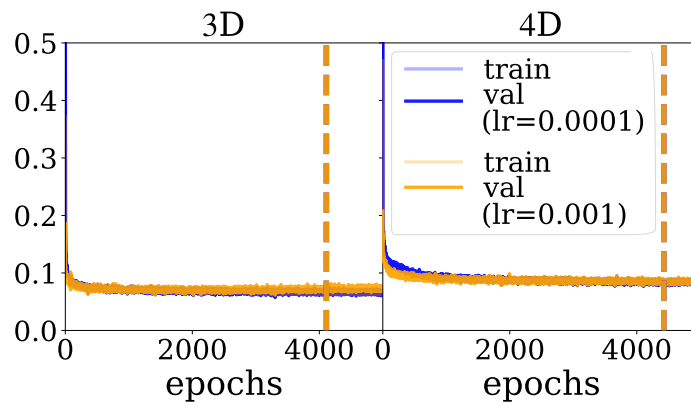


Figure 6: Loss functions for the Jansen & Rit Neural Mass Model obtained for score networks trained over 5 000 epochs with the Adam optimizer, a batch size of 256 and learning rates $lr = 1e^{-3}$ (orange) and $lr = 1e^{-4}$ (blue). The validation loss was computed on a held-out validation set of 20% of the training dataset of size $N_{\text{train}} = 50\,000$. Dashed lines indicate the epoch at early stopping time. The chosen model corresponds to the smallest validation loss, here obtained for a learning rate of $1e^{-4}$.

G Additional results for the toy models

m	Speed up GAUSS	Speed up JAC
2	0.39 ± 0.01	0.56 ± 0.00
4	0.39 ± 0.01	0.55 ± 0.00
8	0.39 ± 0.01	0.56 ± 0.00
10	0.38 ± 0.01	0.52 ± 0.00
16	0.38 ± 0.01	0.54 ± 0.00
32	0.37 ± 0.01	0.52 ± 0.00

Table 2: Confidence intervals for the ratio between elapsed time for each algorithm (GAUSS, JAC) and the equivalent Langevin sampler in the Gaussian case for each tested m . The values are averaged over number of sampling steps, ϵ and n .

Algorithm	N steps	Δt (s)	sW
GAUSS	50	0.99 +/- 0.00	0.30 +/- 0.05
JAC	50	0.89 +/- 0.00	82.73 +/- 67.41
Langevin	50	1.77 +/- 0.01	0.24 +/- 0.01
GAUSS	150	1.83 +/- 0.01	0.31 +/- 0.04
JAC	150	2.66 +/- 0.00	5.89 +/- 1.07
Langevin	150	5.28 +/- 0.01	0.35 +/- 0.02
GAUSS	400	3.91 +/- 0.01	0.31 +/- 0.04
JAC	400	7.13 +/- 0.02	3.41 +/- 1.04
Langevin	400	14.06 +/- 0.04	0.43 +/- 0.02
GAUSS	1000	8.85 +/- 0.03	0.34 +/- 0.03
JAC	1000	17.69 +/- 0.07	7.33 +/- 5.41
Langevin	1000	35.08 +/- 0.15	0.47 +/- 0.02

Table 3: Sliced Wasserstein (sW) distance (normalized) and total elapsed time for the Gaussian Mixture toy problem with $d = 10$, $n = 32$ and $\epsilon = 10^{-2}$ per algorithm and number of generation steps. Mean and std over 5 different seeds.

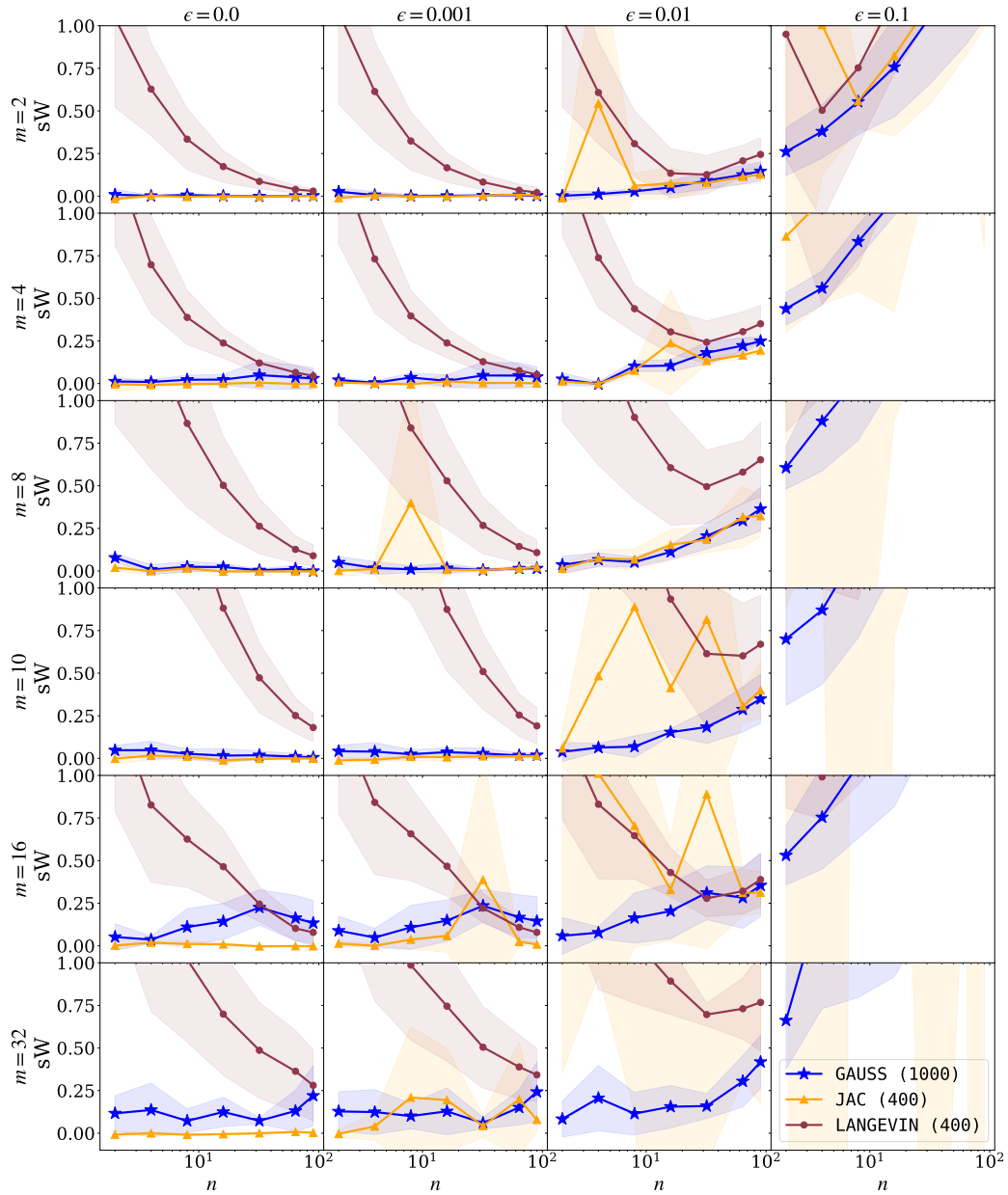


Figure 7: Sliced Wasserstein (sW) distance (normalized) as a function of the number of observations n for **GAUSS**, **JAC** and **LANGEVIN** with different levels of ϵ . Results are shown for the Gaussian example in several dimensions $m \in [2, 4, 8, 10, 16, 32]$. Mean and std over 5 different seeds.

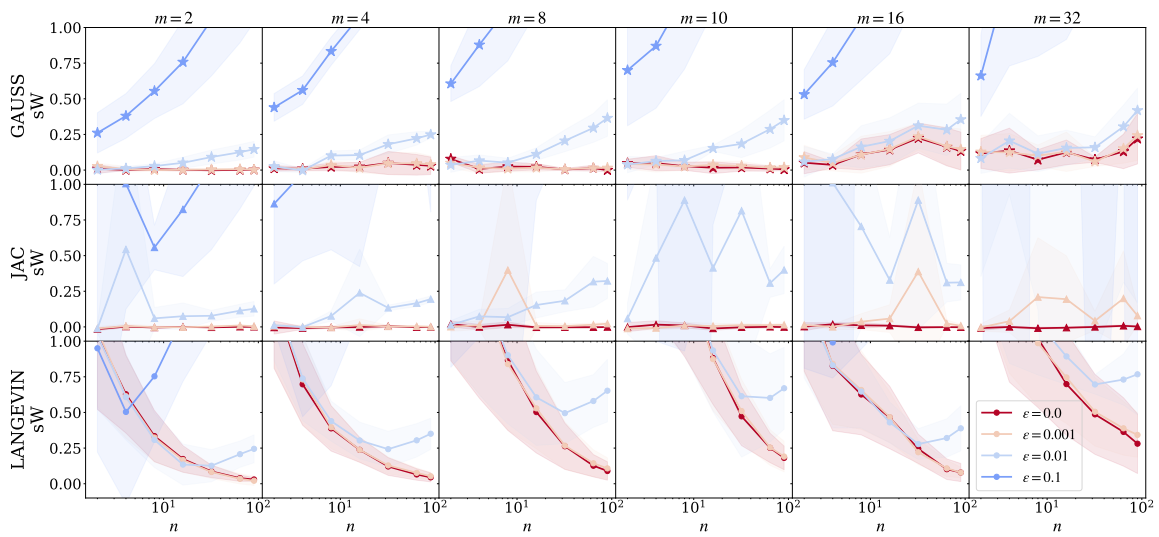


Figure 8: Sliced Wasserstein (sW) distance (normalized) as a function of the number of observations n for the different methods with different levels of ϵ . Results are shown for the Gaussian example in several dimensions $m \in [2, 4, 8, 10, 16, 32]$. Mean and std over 5 different seeds.

H Additional results for SBI benchmarks

We here include more detailed results for the three SBI benchmark tasks from Section 4.2, i.e. for more values of n and additional evaluation metrics. As a complement to the sliced Wasserstein (sW) distance, we report results obtained for the Maximum Mean Discrepancy (MMD) and the Classifier-Two-Sample Test (C2ST) metrics from the `sbibm` package, respectively in Appendix H.2 and H.3. These metrics are less discriminative but highlight an interesting point: Figures 12 and 14 show *increasing MMD and C2ST values for higher n* . This can be explained by the accumulation of approximation errors, as we sum over n evaluations of the score model to obtain the tall posterior score for n observations. We refer the reader to Appendix L.2, which investigates a possible solution to this issue: partially factorized score-based posterior sampling algorithms, such as PF-NPSE proposed by (Geffner et al., 2023).

H.1 Sliced Wasserstein distance

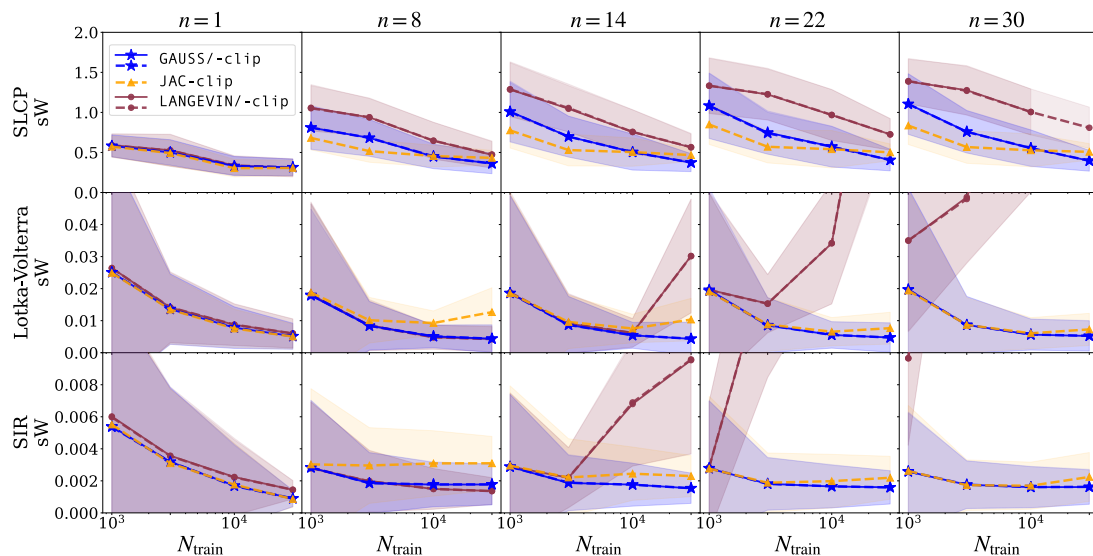


Figure 9: Sliced Wasserstein (sW) as a function of $N_{\text{train}} \in [10^3, 3 \cdot 10^3, 10^4, 3 \cdot 10^4]$ between the samples obtained by each algorithm and the true tall posterior distribution $p(\theta \mid x_{1,n}^*)$ (for $n \in [1, 8, 14, 22, 30]$). Mean and std over 25 different parameters $\theta^* \sim \lambda(\theta)$.

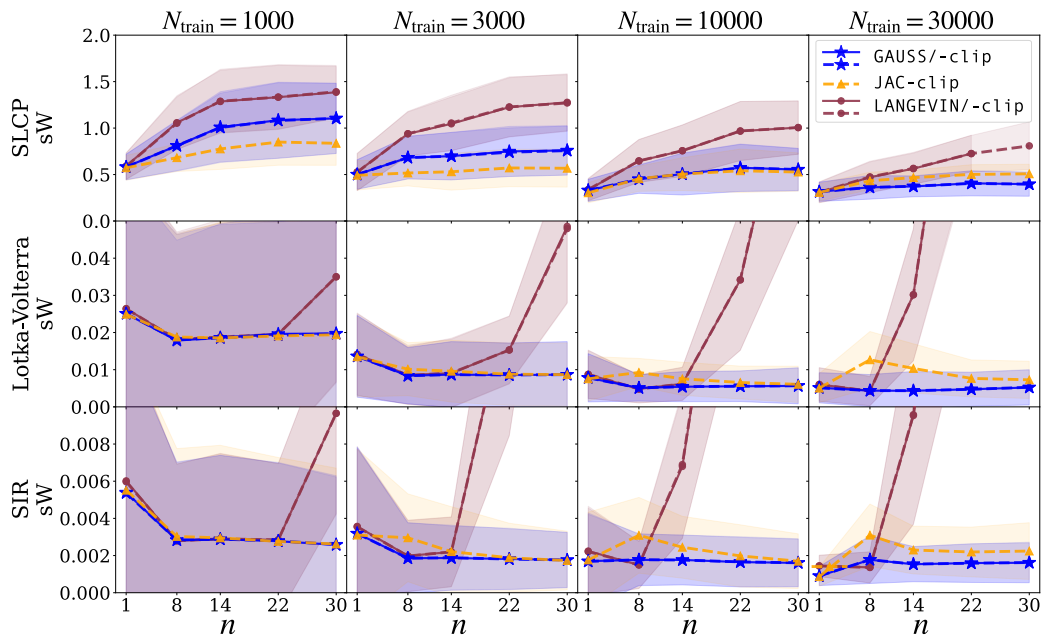


Figure 10: Sliced Wasserstein (sW) a function of $n \in [1, 8, 14, 22, 30]$ between the samples obtained by each algorithm and the true tall posterior distribution $p(\theta \mid x_{1,n}^*)$ (for $N_{\text{train}} \in [10^3, 3.10^3, 10^4, 3.10^4]$). Mean and std over 25 different parameters $\theta^* \sim \lambda(\theta)$.

H.2 Maximum Mean Discrepancy

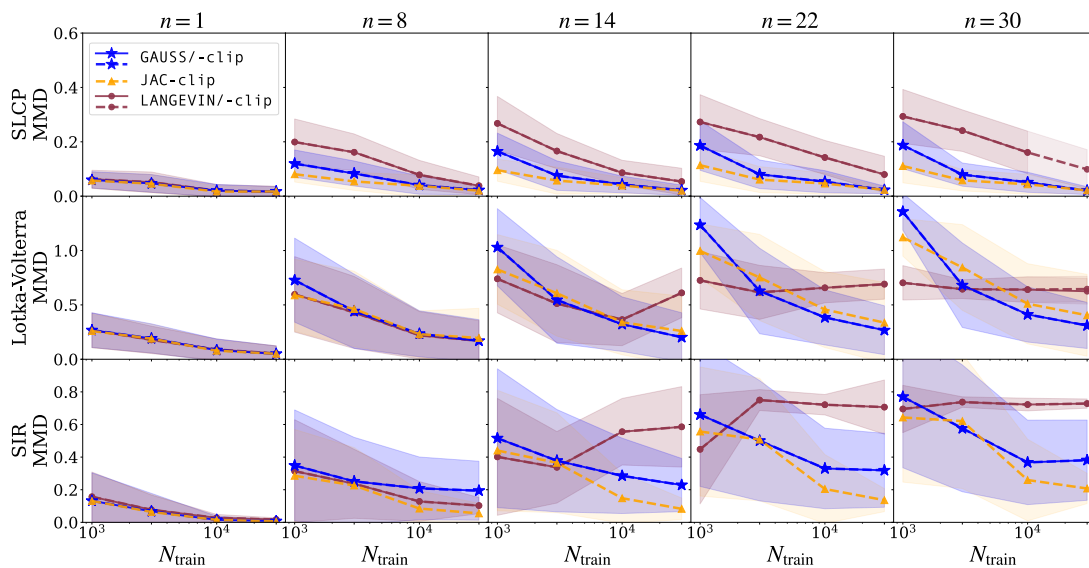


Figure 11: MMD as a function of $N_{\text{train}} \in [10^3, 3 \cdot 10^3, 10^4, 3 \cdot 10^4]$ between the samples obtained by each algorithm and the true tall posterior distribution $p(\theta \mid x_{1,n}^*)$ (for $n \in [1, 8, 14, 22, 30]$). Mean and std over 25 different parameters $\theta^* \sim \lambda(\theta)$.

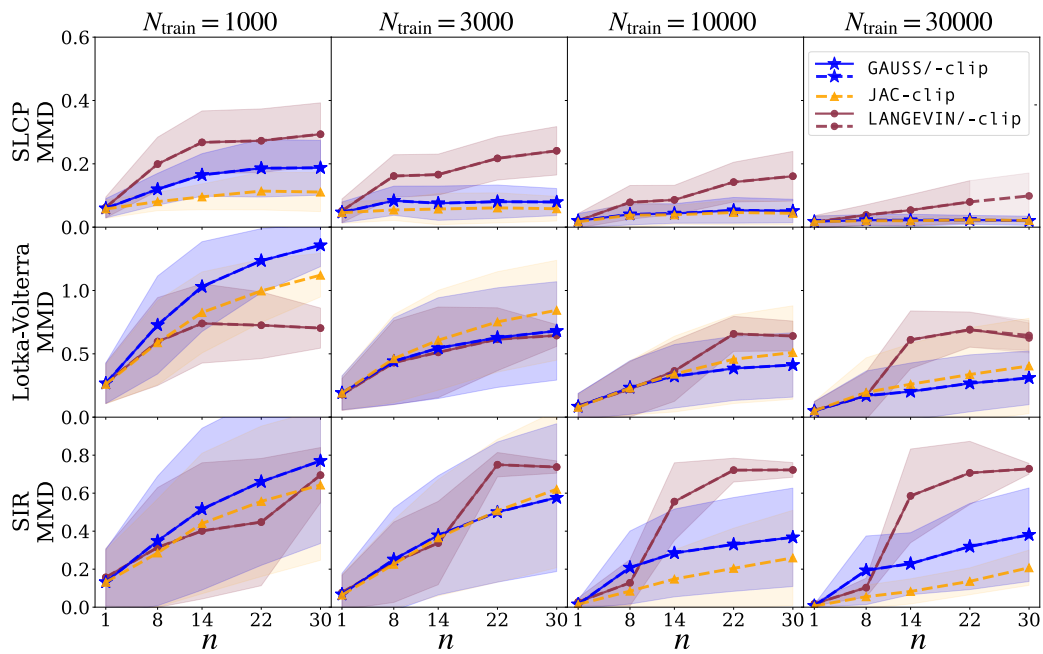


Figure 12: MMD as a function of $n \in [1, 8, 14, 22, 30]$ between the samples obtained by each algorithm and the true tall posterior distribution $p(\theta \mid x_{1,n}^*)$ (for $N_{\text{train}} \in [10^3, 3 \cdot 10^3, 10^4, 3 \cdot 10^4]$). Mean and std over 25 different parameters $\theta^* \sim \lambda(\theta)$.

H.3 Classifier-Two-Sample Test

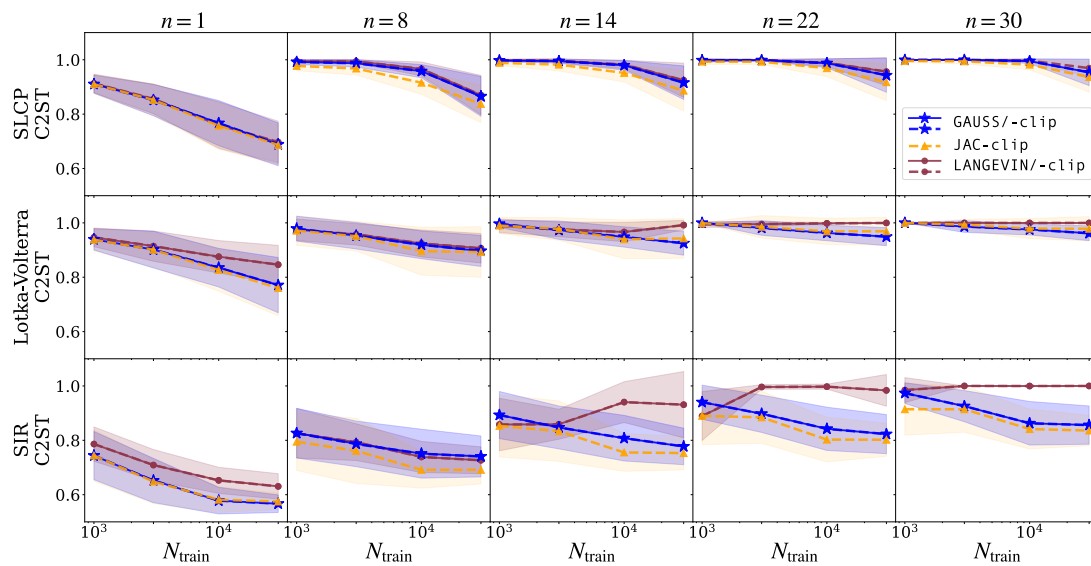


Figure 13: C2ST as a function of $N_{\text{train}} \in [10^3, 3 \cdot 10^3, 10^4, 3 \cdot 10^4]$ between between the samples obtained by each algorithm and the true tall posterior distribution $p(\theta \mid x_{1,n}^*)$ (for $n \in [1, 8, 14, 22, 30]$). Mean and std over 25 different parameters $\theta^* \sim \lambda(\theta)$.

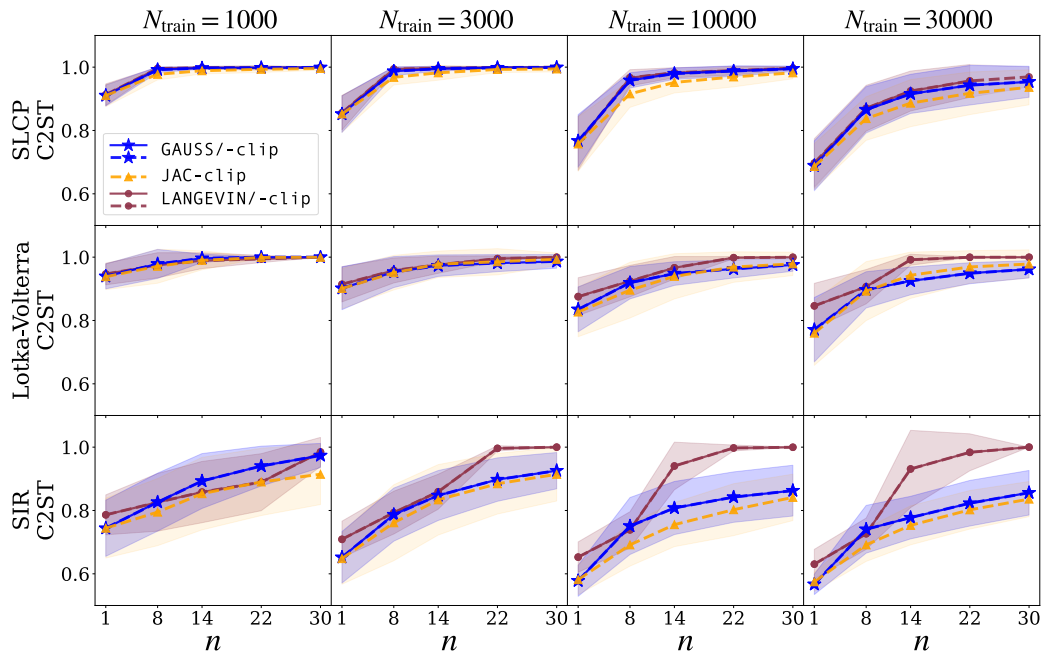


Figure 14: C2ST as a function of $n \in [1, 8, 14, 22, 30]$ between the samples obtained by each algorithm and the true tall posterior distribution $p(\theta \mid x_{1,n}^*)$ (for $N_{\text{train}} \in [10^3, 3 \cdot 10^3, 10^4, 3 \cdot 10^4]$) and the Dirac of the true parameters θ^* used to simulate the observations $x_{1,n}^*$. Mean and std over 25 different parameters $\theta^* \sim \lambda(\theta)$.

I Results for additional tasks from the SBI benchmark

To complete our empirical study, we added results for additional examples from the SBI benchmark (Lueckmann et al., 2021): Gaussian Linear, GMM, GMM (uniform)⁷, B-GLM/ (raw)⁸ and Two Moons. These new results allows us to compare the performance of our proposal on other challenging situations, such as when scaling to highly structured (e.g. multimodal) posteriors and high-dimensional observation spaces. Note that these examples go a step further as compared to the experiments carried out by Geffner et al. (2023), including non-Gaussian priors⁹. Figures 15, 16 and 17 respectively report the sW, MMD and C2ST as a function of N_{train} . They all show that our algorithm outperforms the Langevin sampler, with smaller distance values everywhere but for the GMM (uniform) example. Interestingly, the certainly very discriminative C2ST metric, shows that all three algorithms fail to infer the tall posterior for the Two Moons and B-GLM/ (raw) examples.

⁷same as GMM but with a Uniform prior.

⁸Bernoulli GLM with summary statics / high dimensional raw data.

⁹Note that this was already the case for SLCP with Uniform prior.

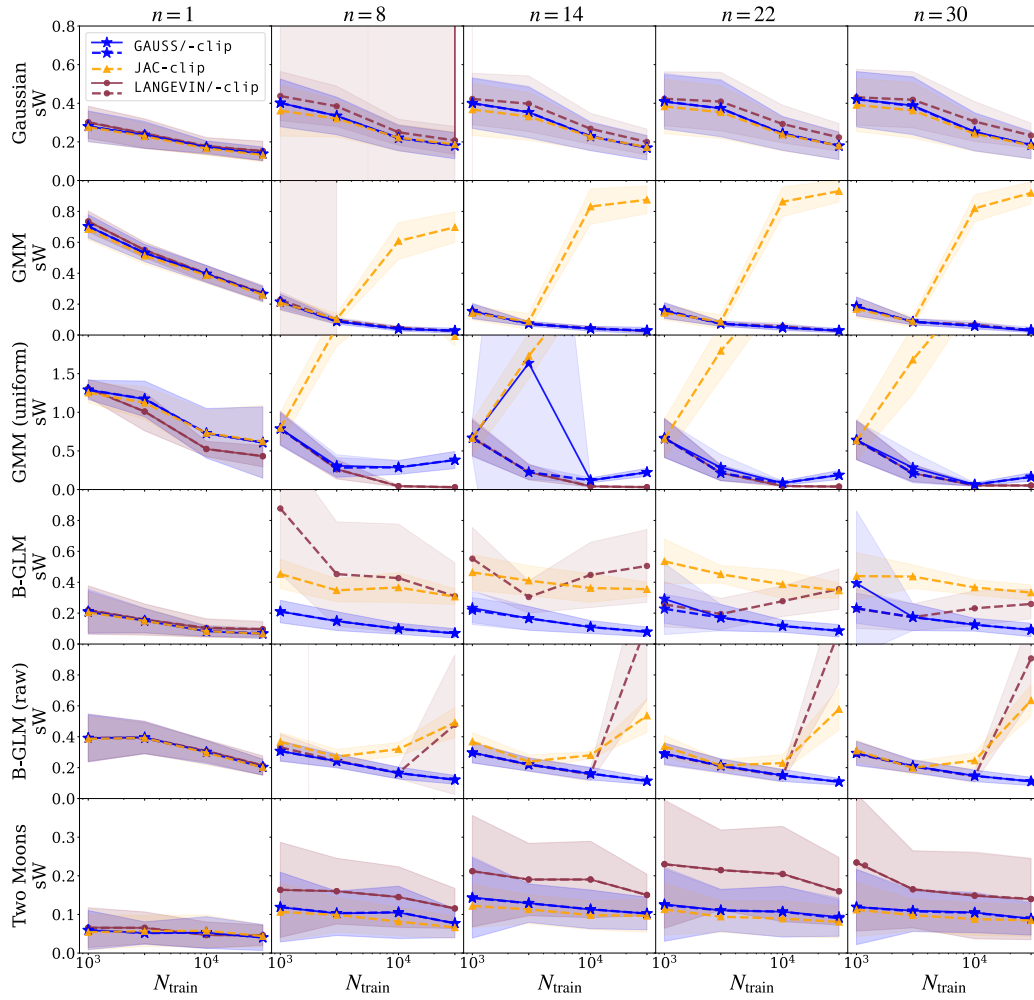


Figure 15: Sliced Wasserstein (sW) distance as a function of $N_{\text{train}} \in [10^3, 3 \cdot 10^3, 10^4, 3 \cdot 10^4]$ between the samples obtained by each algorithm and the true target posterior distribution $p(\theta \mid x_{1,n}^*)$ (for $n \in [1, 8, 14, 22, 30]$). Mean and std over 25 different parameters $\theta^* \sim \lambda(\theta)$.

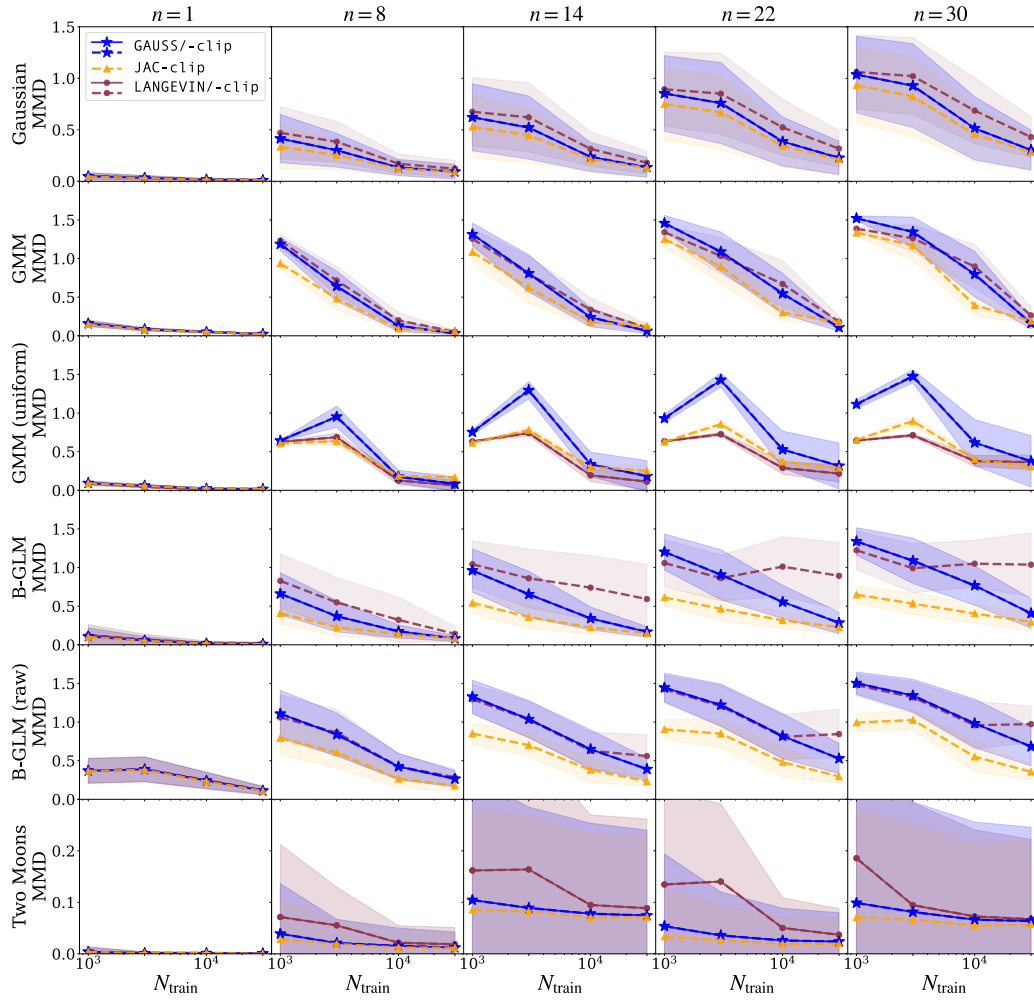


Figure 16: MMD as a function of $N_{\text{train}} \in [10^3, 3.10^3, 10^4, 3.10^4]$ between between the samples obtained by each algorithm and the true tall posterior distribution $p(\theta \mid x_{1,n}^*)$ (for $n \in [1, 8, 14, 22, 30]$). Mean and std over 25 different parameters $\theta^* \sim \lambda(\theta)$.

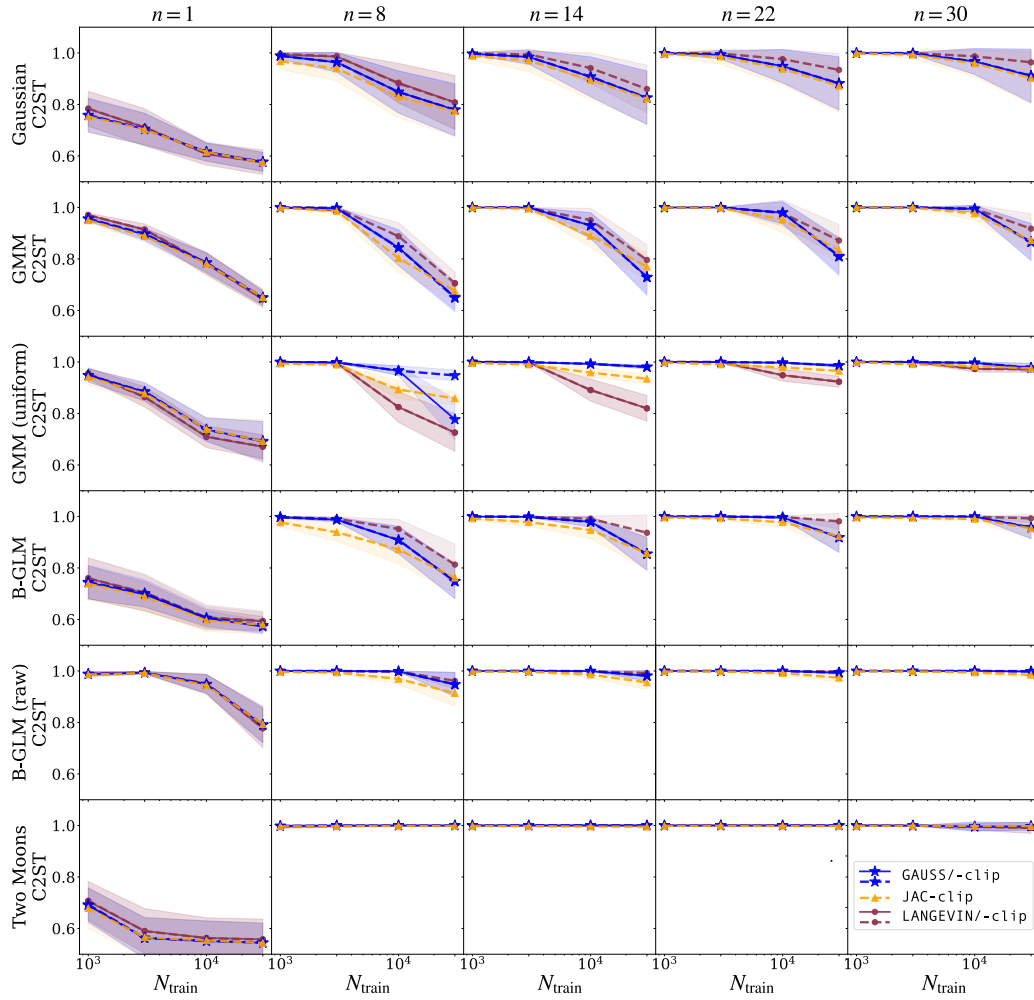


Figure 17: C2ST as a function of $N_{\text{train}} \in [10^3, 3.10^3, 10^4, 3.10^4]$ between between the samples obtained by each algorithm and the true tall posterior distribution $p(\theta \mid x_{1,n}^*)$ (for $n \in [1, 8, 14, 22, 30]$). Mean and std over 25 different parameters $\theta^* \sim \lambda(\theta)$.

J Results for the Jansen-Rit Neural Mass Model

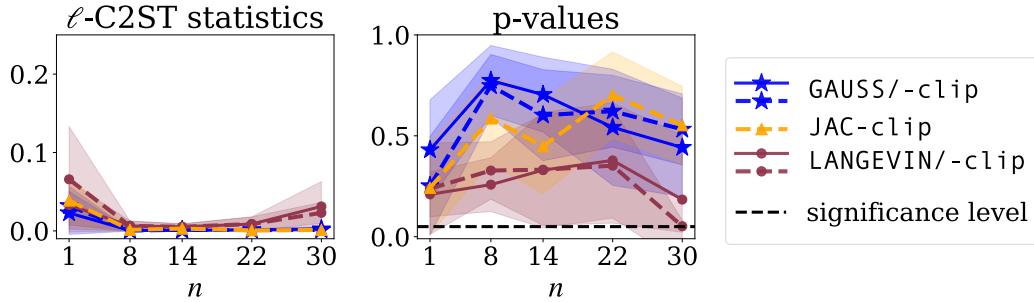
In this section, we report results obtained for the simplified version (3D) and the full (4D) Jansen and Rit Neural Mass Model (JRNMM).

In both cases, we first evaluate the accuracy of each posterior sampling algorithms (**GAUSS**, **JAC** and **LANGEVIN**) w.r.t. the true tall posterior, using the *local* Classifier-Two-sample Test (ℓ -C2ST) diagnostic proposed by Linhart et al. (2023) and implemented in the `sbi` toolbox. ℓ -C2ST is a frequentist hypothesis test that evaluates the null hypothesis of sample equality between two conditional distributions by training a classifier on data from the respective joint distributions. The test statistic takes values in $[0, 0.25]$ and is defined by the mean squared error (MSE) between the predicted class probabilities and one half, i.e. the chance level where the classifier is unable to distinguish between the two data classes. Higher MSE values indicate more distributional differences.

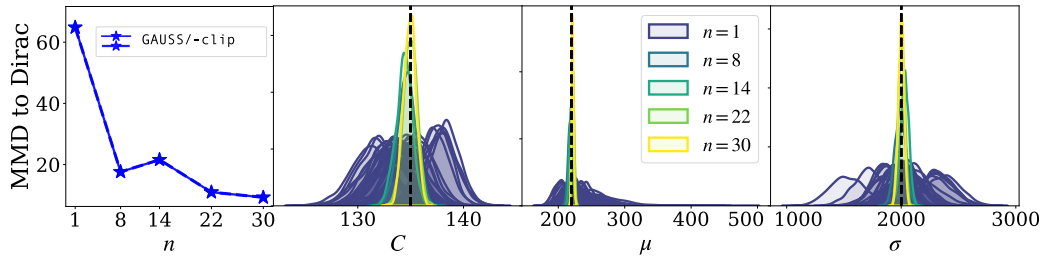
Figures 18a and 19a respectively show the ℓ -C2ST results for the 3D and 4D JRNMM cases, obtained using the `MLPClassifier` from `scikit-learn`, with default parameters from the `sbi` implementation and trained using 10 000 samples $(\Theta_i, X_{i,1:n})$ from the joint distributions corresponding to the estimated and true tall data posteriors. We report the mean and std over 5 different seeds used for the initialization of the classifier. On the left, we plot the ℓ -C2ST statistics, computed on 10 000 samples of the approximate posterior obtained by each sampling algorithms for a given observation set $x_{1:n}^* \sim p(\cdot)$. On the right, we display the associated p-values computed by comparing the obtained statistics to the null hypothesis, estimated over 100 trials. In both cases, the **GAUSS** algorithm consistently yields test statistics close to 0 and p-values above the significance level set at $\alpha = 0.05$, which means that there is no evidence that the estimated posterior is not statistically consistent with the true tall posterior at $x_{1:n}^*$. This is not the case for **JAC**, whose un-clipped version yields MSE values outside the plot limits and **LANGEVIN**, for which the test is more easily rejected in the 3D case (large std on pvalues that overlap with the significance level) and very clearly rejected in the 4D case for $n > 14$ (p-value below the significance level).

In a second time, we evaluate the the ability of our tall posterior to concentrate around the true parameters θ^* generating observations $x_1, \dots, x_n \sim p(x \mid \theta^*)$ as n increases. This is quantified using the Maximum Mean Discrepancy (MMD) between the posterior marginals and the Dirac distribution δ_{θ^*} , computed on 10 000 samples obtained with **GAUSS**.

Figures 18b and 19b respectively show the results for the 3D and 4D JRNMM cases. On the left, we plot the MMD as a function of the number n of observations. On the right are displayed the marginals corresponding to the posterior samples obtained with **GAUSS** for observation sets $x_{1:n}^*$ of increasing size. For the 3D case we observe, a progressive concentration around θ^* , with sharper posterior marginals and decreasing MMD. For the 4D JRNMM, the tall posterior takes a “sharpened banana” shape: while it is able to concentrate around (C, g) , the dispersion along the dimensions of (μ, σ) is sustained.

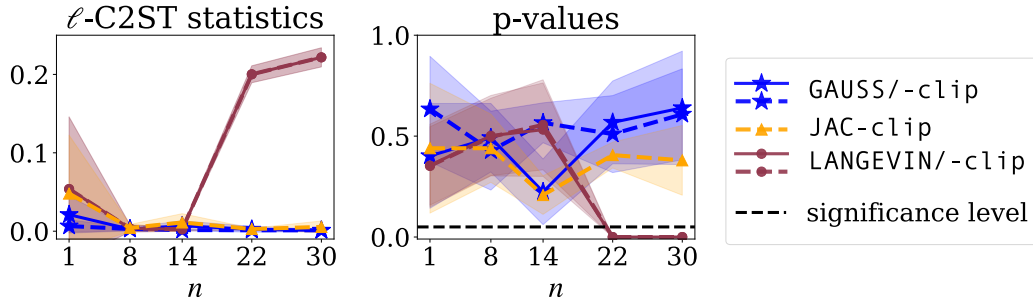


(a) **Accuracy of the sampling algorithms w.r.t. the true tall posterior.** We show ℓ -C2ST statistics (left) and corresponding p-values (right) computed for samples obtained with **GAUSS**, **JAC** and **LANGEVIN** at $x_{1:n}^*$ for $n \in [1, 8, 14, 22, 30]$. Mean and std over 5 seeds.

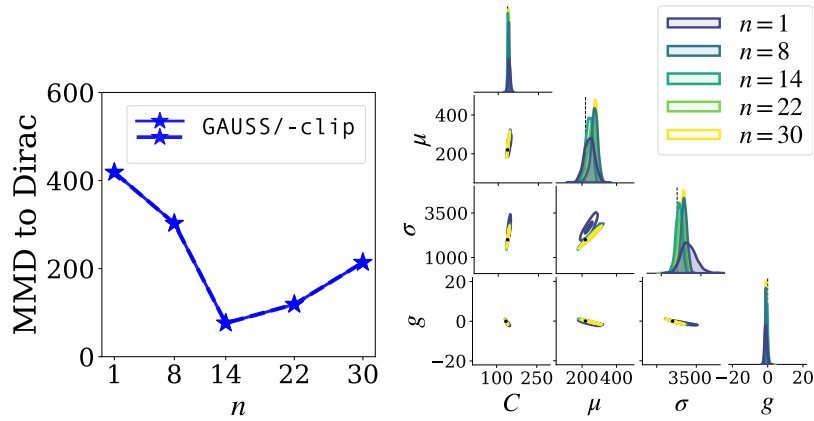


(b) **Concentration of the tall posterior.** Left: MMD between the marginals of the approximate posterior obtained with **GAUSS** and the Dirac of the true parameters $\theta^* = (125, 220, 2000)$ (black dashed lines) used to simulate the observations $x_{1:n}^*$. Right: Histograms of the 1D marginals of the posterior samples obtained with **GAUSS** for 30 single observations x_1^*, \dots, x_{30}^* ($n = 1$) and for observation sets $x_{1:n}^*$ of increasing size.

Figure 18: Inference on the 3D JRNMM (fixed $g = 0$).



(a) **Accuracy of the sampling algorithms w.r.t. the true tall posterior.** We show ℓ -C2ST statistics (left) and corresponding p-values (right) computed for **GAUSS**, **JAC** and **LANGEVIN** at $x_{1:n}^*$ for $n \in [1, 8, 14, 22, 30]$. Mean and std over 5 seeds.



(b) **Concentration of the tall posterior.** Left: MMD between the marginals of the approximate posterior obtained with **GAUSS** and the Dirac of the true parameters $\theta^* = (125, 220, 2000, 0)$ (black dashed lines) used to simulate the observations $x_{1:n}^*$. Right: Histograms of the 1D and 2D marginals of the posterior samples obtained with **GAUSS** for a single observations x^* ($n = 1$) and for observation sets $x_{1:n}^*$ of increasing size.

Figure 19: Inference on the full (4D) JRNMM.

K Limitations of Langevin sampling

Sensitivity to the quality of the score model. Our results in Section 4.1 analyze the robustness of the different sampling algorithms and essentially show that the Langevin algorithm is very sensitive to noisy score networks.

Step-size choice. We found that different step sizes can generate very different results for a given score model. We have added in Figure 20 a comparison between the original ULA (Unadjusted Langevin algorithm) used in (Geffner et al., 2023) and an additional implementation with "tamed" step sizes from (Brosse et al., 2017), which is known to stabilize ULA. We can see that the same choice of hyper-parameters for the "Geffner setting" leads to different behaviour with increasing n . Namely, the learning rate in the ULA algorithm seems to be too large (i.e. not enough steps are done) in settings with big n . We can see that the stabilization tools from the tamed version yield a more stable ULA algorithm but that does not provide a completely satisfying solution. Fundamentally, there exists a setting where the Langevin algorithm will work (taking a small enough learning rate for a long enough time), but this setting is extremely dependent of the problem at hand. This is precisely the strength of our algorithm when compared to ULA: we do not need to sample several times for each marginal p_t at each time step t . Note that unfortunately, the code for (Geffner et al., 2023) is not available, so our results are based in a best-effort attempt to reproduce the proposed algorithm.

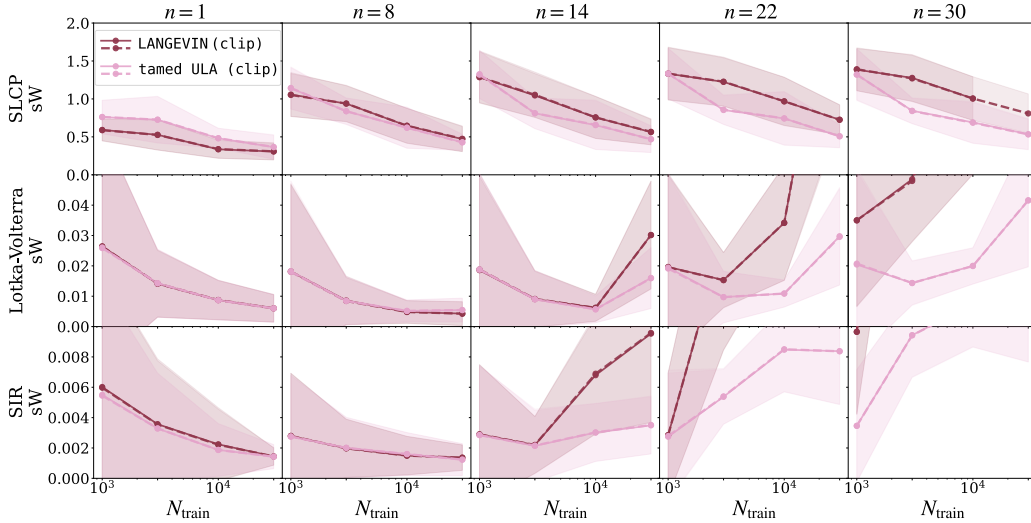


Figure 20: Comparison between the LANGEVIN algorithm from (Geffner et al., 2023) (used in all our experiments) and a more stable tamed ULA version with "tamed" step size from (Brosse et al., 2017). The plots show the sliced Wasserstein (sW) w.r.t. the true tall posterior $p(\theta \mid x_{1:n}^*)$ as a function of $N_{\text{train}} \in \{10^3, 3 \cdot 10^3, 10^4, 3 \cdot 10^4\}$ and for $n \in \{1, 8, 14, 22, 30\}$.

L Beyond the proposal: Classifier-free guidance and Partial Factorization

The implementation of both of these extension can be found in our Code repository¹⁰. Their performance was investigated on the three benchmarks Lotka-Volterra, SLCP and SIR.

L.1 Classifier-free guidance (CFG).

It is possible to implicitly learn the prior score via the classifier-free guidance approach (Ho and Salimans, 2021), which essentially consists in randomly dropping the context variables when training the posterior score model (e.g. 20% of the time). This is useful in cases where the diffused prior score cannot be computed analytically. Figure 21 displays the sliced Wasserstein (sW) distance as a function of N_{train} and compares the results obtained when using our proposition with the learned vs. the analytical prior score (resp. GAUSS (CFG) vs. GAUSS). We also report the results obtained Maximum Mean Discrepancy (MMD) and Classifier-Two-Sample Test (C2ST) accuracy respectively in Figures 22 and 23. The results are highly accurate for the Log-Normal priors of Lotka-Volterra and SIR, but less satisfying for the Uniform prior in SLCP. We think that this is caused by the discontinuities of the Uniform distribution. In summary, it seems that (under some smoothness assumptions) it is indeed possible to learn the prior score via the classifier-free guidance approach.

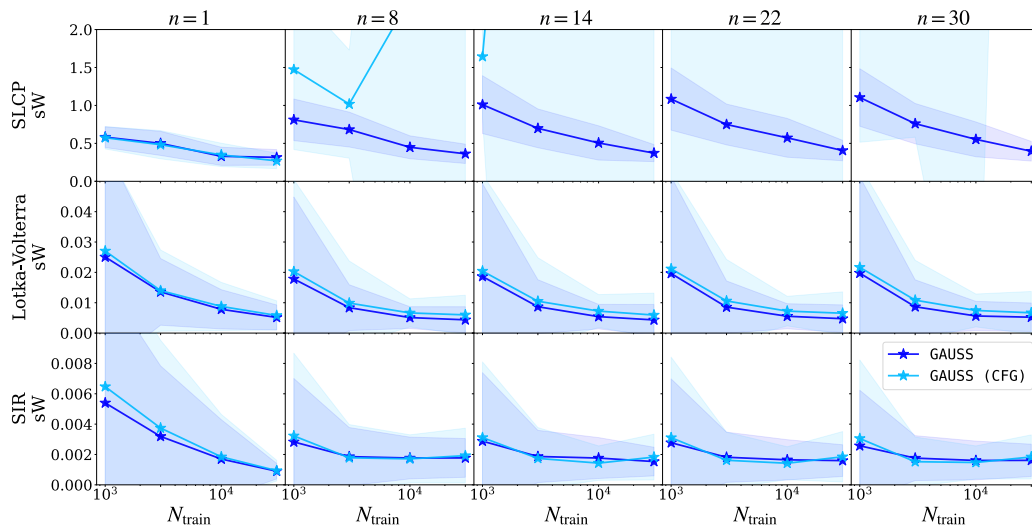


Figure 21: Sliced Wasserstein (sW) distance w.r.t. the true tall posterior $p(\theta | x_{1:n}^*)$ as a function of $N_{\text{train}} \in \{10^3, 3.10^3, 10^4, 3.10^4\}$ and for $n \in \{1, 8, 14, 22, 30\}$. Comparison between the results obtained with our algorithm when combined with the analytical prior score and the one learned via classifier-free guidance (resp. GAUSS and GAUSS (CFG)).

¹⁰<https://github.com/JuliaLinhart/diffusions-for-sbi>

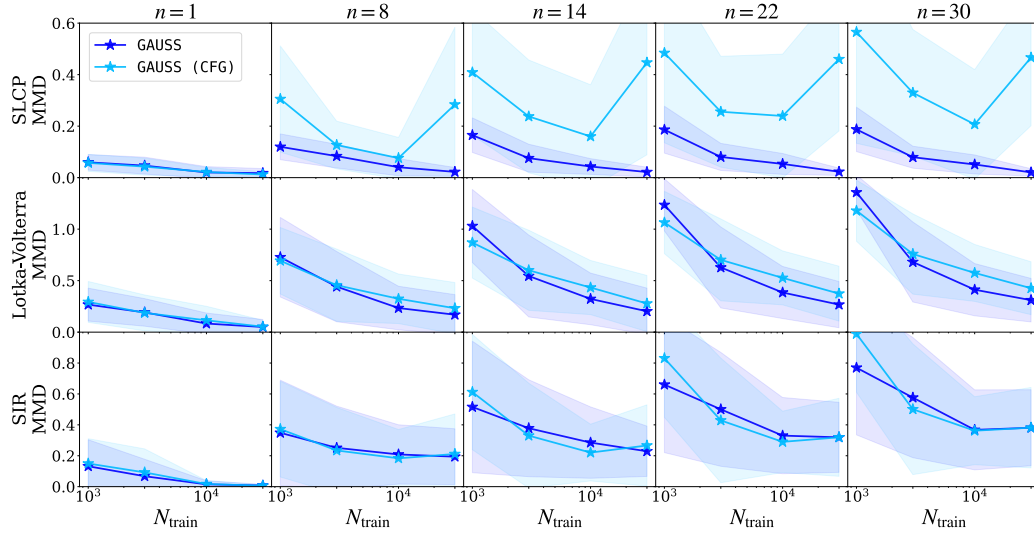


Figure 22: Maximum Mean Discrepancy (MMD) w.r.t. the true tall posterior $p(\theta \mid x_{1:n}^*)$ as a function of $N_{\text{train}} \in \{10^3, 3 \cdot 10^3, 10^4, 3 \cdot 10^4\}$ and for $n \in \{1, 8, 14, 22, 30\}$. Comparison between the results obtained with our algorithm when combined with the analytical prior score and the one *learned via classifier-free guidance* (resp. GAUSS and GAUSS (CFG)).

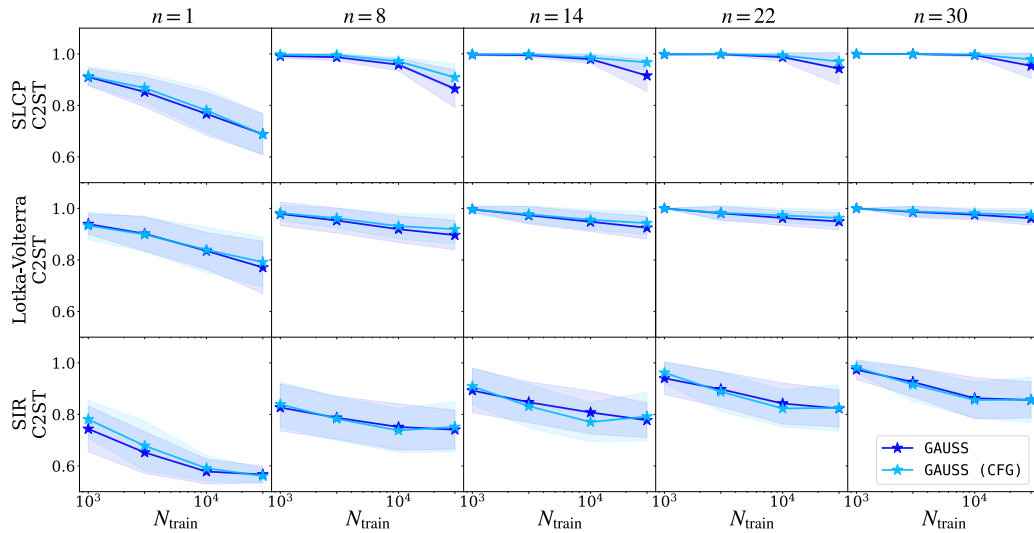


Figure 23: Classifier-Two-Sample Test (C2ST) accuracy w.r.t. the true tall posterior $p(\theta \mid x_{1:n}^*)$ as a function of $N_{\text{train}} \in \{10^3, 3 \cdot 10^3, 10^4, 3 \cdot 10^4\}$ and for $n \in \{1, 8, 14, 22, 30\}$. Comparison between the results obtained with our algorithm when combined with the analytical prior score and the one *learned via classifier-free guidance* (resp. GAUSS and GAUSS (CFG)).

L.2 Partial factorization (PF-NPSE).

In the same way as in (Geffner et al., 2023), our proposed algorithm can naturally be extended to a partially factorized version. Specifically, it consists in approximating the tall posterior by factorizing it over batches of context observations (instead of a single x). To do so, the score model is modified to take as input context sets with variable sizes (between 1 and n_{\max}). The given sampling algorithm (e.g. GAUSS, LANGEVIN) is then modified to split the context observations x_1^*, \dots, x_n^* into subsets of smaller size $k < n_{\max} < n$, before passing them to the trained score model. This approach should allow for a good trade-off between the accumulation of approximation errors due to multiple evaluations of the score model (n/n_{\max} times) and the increased simulation budget ($\times n_{\max}$). This approach should allow for a good trade-off between the accumulation of approximation errors due to multiple evaluations of the score model (n/n_{\max} times) and the increased simulation budget ($\times n_{\max}$).

We investigated the performance of PF-NPSE on the SBI benchmarks (Lotka-Volterra, SIR and SLCP). For each of the three examples we trained a PF-NPSE model targeting the score models for the law of θ given $x_{1:n_{\max}}$ for $n_{\max} \in \{1, 3, 6, 30\}$. Figure 24 displays the sliced Wasserstein (sW), Maximum Mean Discrepancy (MMD) and the Classifier-Two-Sample Test (C2ST) accuracy for $n = 30$ observations as a function of the N_{train} for samples obtained with the partially factorized LANGEVIN and GAUSS samplers and for all n_{\max} . The extreme case $n_{\max} = 1$ corresponds to the original "fully" factorized version of the samplers. $n_{\max} = n = 30$ correspond to the other extreme case with no factorization, but maximum simulation budget. We can see that the optimal sW values lie in the middle of the spectrum (i.e. for $n_{\max} = 3, 6$), which corresponds to what was concluded in (Geffner et al., 2023). Note that the performance of LANGEVIN is drastically improved for $n_{\max} > 1$, while GAUSS all results are close. In any case, the results suggests that a practitioner will gain in choosing (a small enough) $n_{\max} > 1$.

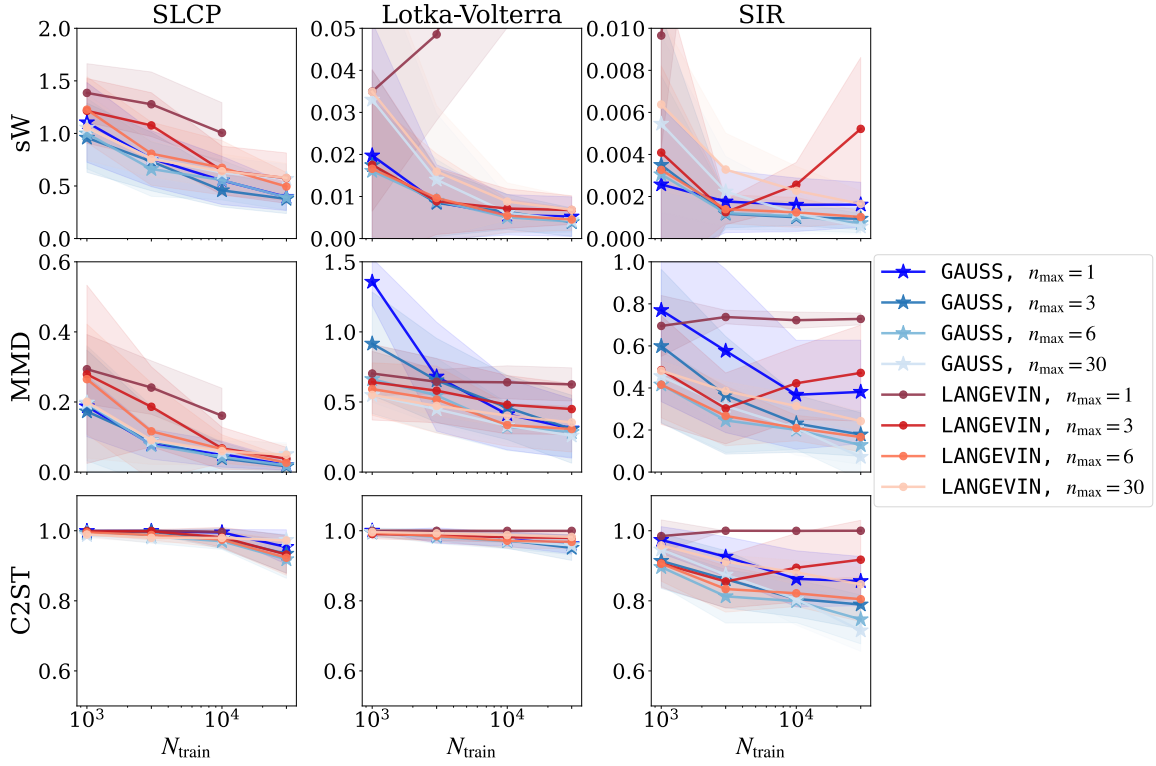


Figure 24: Results obtained with the *partially factorized* LANGEVIN and GAUSS samplers to infer the tall posterior conditioned on a total number of observations $n = 30$, for $n_{\max} = 1, 3, 6, 30$. We report the sliced Wasserstein (sW), Maximum Mean Discrepancy (MMD) and the Classifier-Two-Sample Test (C2ST) accuracy w.r.t. the true tall posterior $p(\theta \mid x_{1:n}^*)$ as a function of $N_{\text{train}} \in \{10^3, 3 \cdot 10^3, 10^4, 3 \cdot 10^4\}$. The extreme case $n_{\max} = 1$ corresponds to the original "fully" factorized version of the samplers. $n_{\max} = n = 30$ correspond to the other extreme case with no factorization, but maximum simulation budget. We can see that the optimal distance values lie in the middle of this spectrum (i.e. for $n_{\max} = 3, 6$).